



Review

# Recent Developments of Tin (II) Sulfide/Carbon Composites for Achieving High-Performance Lithium Ion Batteries: A Critical Review

Sharif Tasnim Mahmud<sup>1</sup>, Rony Mia<sup>2,3</sup> , Sakil Mahmud<sup>2</sup> , Sha Sha<sup>1</sup>, Ruquan Zhang<sup>1</sup>, Zhongmin Deng<sup>1</sup>, Meltem Yanilmaz<sup>4</sup> , Lei Luo<sup>1,\*</sup> and Jiadeng Zhu<sup>5,\*</sup>

<sup>1</sup> State Key Laboratory of New Textile Materials and Advanced Processing Technology, School of Textile Science and Engineering, Wuhan Textile University, Wuhan 430200, China; tasnimmahmud13047@gmail.com (S.T.M.); shasha@wtu.edu.cn (S.S.); zhangruquan@wtu.edu.cn (R.Z.); zmdeng@wtu.edu.cn (Z.D.)

<sup>2</sup> Hubei Key Laboratory of Biomass Fibers and Eco-Dyeing & Finishing, School of Chemistry and Chemical Engineering, Wuhan Textile University, Wuhan 430200, China; mroni\_mia@yahoo.com (R.M.); sakilmahmud1105@gmail.com (S.M.)

<sup>3</sup> Department of Chemical Engineering, Inha University, Incheon 22212, Korea

<sup>4</sup> Department of Textile Engineering, Istanbul Technical University, Istanbul 34469, Turkey; yanilmaz@itu.edu.tr

<sup>5</sup> Chemical Sciences Division, Oak Ridge National Laboratory, Oak Ridge, TN 37831, USA

\* Correspondence: leiluo@wtu.edu.cn (L.L.); zhujadeng@gmail.com (J.Z.)

**Abstract:** The ever-increasing worldwide energy demand and the limited resources of fossil have forced the urgent adoption of renewable energy sources. Additionally, concerns over CO<sub>2</sub> emissions and potential increases in fuel prices have boosted technical efforts to make hybrid and electric vehicles more accessible to the public. Rechargeable batteries are undoubtedly a key player in this regard, especially lithium ion batteries (LIBs), which have high power capacity, a fast charge/discharge rate, and good cycle stability, while their further energy density improvement has been severely limited, because of the relatively low theoretical capacity of the graphite anode material which is mostly used. Among various high-capacity anode candidates, tin (II) sulfide (SnS<sub>2</sub>) has been attracted remarkable attention for high-energy LIBs due to its enormous resource and simplicity of synthesis, in addition to its high theoretical capacity. However, SnS<sub>2</sub> has poor intrinsic conductivity, a big volume transition, and a low initial Coulombic efficiency, resulting in a short lifespan. SnS<sub>2</sub>/carbon composites have been considered to be a most promising approach to addressing the abovementioned issues. Therefore, this review summarizes the current progress in the synthesis of SnS<sub>2</sub>/carbon anode materials and their Li-ion storage properties, with special attention to the developments in Li-based technology, attributed to its immense current importance and promising prospects. Finally, the existing challenges within this field are presented, and potential opportunities are discussed.

**Keywords:** tin (II) sulfide; carbon; lithium ion battery; anode; lithium storage property; high energy density



**Citation:** Mahmud, S.T.; Mia, R.; Mahmud, S.; Sha, S.; Zhang, R.; Deng, Z.; Yanilmaz, M.; Luo, L.; Zhu, J. Recent Developments of Tin (II) Sulfide/Carbon Composites for Achieving High-Performance Lithium Ion Batteries: A Critical Review. *Nanomaterials* **2022**, *12*, 1246. <https://doi.org/10.3390/nano12081246>

Academic Editor: Jung Woo Lee

Received: 8 February 2022

Accepted: 5 April 2022

Published: 7 April 2022

**Publisher's Note:** MDPI stays neutral with regard to jurisdictional claims in published maps and institutional affiliations.



**Copyright:** © 2022 by the authors. Licensee MDPI, Basel, Switzerland. This article is an open access article distributed under the terms and conditions of the Creative Commons Attribution (CC BY) license (<https://creativecommons.org/licenses/by/4.0/>).

## 1. Introduction

Lithium ion batteries (LIBs), with high energy density, extended cycle life, and environmental friendliness, have been considered to be one of the most appealing energy storage systems, and have played an increasingly significant role in modern civilization [1–6]. The progressing advancement of LIBs has brought exceptional enhancements in different parts of their activity [7–12], being widely involved on the market of compact electronic devices (e.g., cell phones, workstations, advanced cameras, etc.). Additionally, they have been distinguished as the favored force hotspot for electric vehicles (EVs) and fixed-vitality energy storage. However, state-of-the-art LIBs cannot fulfill the developing need for EVs and huge scope vitality energy storage [13–17], which is mainly caused by the limited capacity (372 mAh/g) of the mostly used graphite anode [13,14,17–21]. Thus, tremendous

efforts have been made to fabricate high-capacity anode materials, including elementary substances (i.e., Ge, P, Sb, Si), transition metal oxides (i.e., MnO, V<sub>2</sub>O<sub>5</sub>), metal sulfides (i.e., ZnS, Cu<sub>2</sub>S), etc. [22–42]. Among them, SnS<sub>2</sub> has been attracted remarkable attention because of its low cost, environmental friendliness, and high theoretical specific capacity [43–47]. SnS<sub>2</sub> has the catenation ability of sulfur and contributes to the enrichment of the chemistry of tin sulfide. It is also possible to include other elements (metal and non-metal) to form trivalent and quadratic tin sulfide structures, as well as ternary and quaternary materials [48–52].

For SnS<sub>2</sub>, tin particles can exist in various oxidation states and different coordination structures, and sulfur ions have an enormous electronegativity and solid polarizability [16,53–57]. Li-ions diffuse from the octahedral gap position, where the energy is most supported, to the adjacent octahedral gap position, through the tetrahedral gap position. The expansion of the layer spacing is beneficial for reducing the diffusion barrier [58,59]. In addition, the energy density of SnS<sub>2</sub>-based LIBs can reach as high as 286 Wh/kg, which is much better than those of commercial graphite [60]. Despite these advantages, SnS<sub>2</sub> has certain drawbacks that hinder its broad application, such as the non-negligible volume change issue and the comparatively poor initial Coulombic efficiency (CE), which is related to the irreversible synthesis of Li<sub>2</sub>S and Li<sub>x</sub>SnS<sub>2</sub> [61–63].

Overall, the commercial applications of SnS<sub>2</sub>-based anode materials are currently limited in large part by the following issues: (1) significant initial irreversible capacity loss as a result of the creation of thick solid electrolyte interphase (SEI) throughout the cycling process; (2) the large volume change that occurs during the charge/discharge process, which results in electrode pulverization and the loss of electrical contact with the current collector, leading to fast capacity fading along with poor cycling performance [64–67]. Many efforts have recently been concentrated on addressing the aforementioned difficulties, as well as advancing the use of SnS<sub>2</sub>-based anode materials in LIBs for practical applications. It has been found that hybridizing SnS<sub>2</sub> with other materials—including nanocarbon [68,69], graphene [70,71], and MXene [72]—or doping SnS<sub>2</sub> with other additives—such as Co [39], Ce [73], Mo [74], etc.—can significantly improve the overall conductivity and structural resilience of SnS<sub>2</sub>-based electrodes, thus resolving the issues mentioned above. As most commonly modified materials, carbon materials (i.e., amorphous carbon, carbon nanotubes, graphene, etc.) have been extensively explored because they can improve the electrical conductivity of the electrode, and can reduce the particle agglomeration of active materials, enhancing the utilization of active materials and extending their lifespan [75–78].

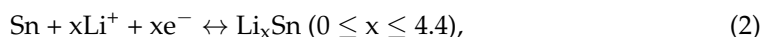
This paper has reviewed the most recent developments in SnS<sub>2</sub>/carbon anodes for LIBs. The structural properties of different composites using SnS<sub>2</sub> clearly demonstrate the importance of preparation process. To fully use all the potential advantages of SnS<sub>2</sub> in LIBs, endeavors have been made to handle the previously mentioned issues and push SnS<sub>2</sub>-based anode materials to handy applications. The morphological design and fabrication of electrode materials tremendously affect the electrochemical performance of LIBs; thus, the large-scale study of those material-based anodes is essential. This review highlights the most recent developments with thorough discussion in the microstructure, morphology, rational synthesis, and electrochemical performance of SnS<sub>2</sub>-based anode materials in LIBs with a goal to provide more insights in this area. The future challenges and research directions for practical, advanced SnS<sub>2</sub>-based anodes are also proposed at the end.

## 2. Working Mechanisms of SnS<sub>2</sub>-Based Anodes in LIBs

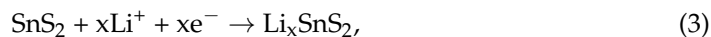
During the past decades, Sn-based materials, particularly SnS<sub>2</sub>, have played a major role in LIBs due to their layered structure, which allows them to provide optimum space for Li-ion intercalation [79–83]. It has also been demonstrated that the advantage of having layers in the structure of the crystal can be used to accommodate Li-ions [84]. The neighboring sulfur layers in SnS<sub>2</sub> are held together by weak van der Waals contacts [85]. The lithiation procedure of SnS<sub>2</sub> can be separated into two phases. When the Li content (*x* in Li<sub>*x*</sub>SnS<sub>2</sub>) is under 1, the volume extension is not remarkable, and only the S particles trap electrons from

Li-ions. When the Li content is more than 1, the  $\text{Sn}^{4+}$  cations are fundamentally decreased, the 3 S-Sn-S layers deteriorate bit by bit, and an  $\text{Li}_x\text{S}_2$  ( $1 \leq x \leq 3$ ) layer is framed between the 2 Sn monolayers, and the volume expansion of  $\text{SnS}_2$  subtly reduces the intensity of Li 2p states. The anode's stability may be jeopardized due to the lithiation-induced volume expansion and crystal structural change. During lithiation/delithiation, Sn-based anode materials always experience 200–300% volume expansion [61–63].

It has been proposed that the electrochemical reaction mechanisms of  $\text{SnS}_2$  with Li-ions are presented in Equations (1) and (2) [86]:



The high theoretical capacity of 645 mAh/g is derived from the reversible reaction (1) of Sn in  $\text{SnS}_2$  with 4.4 mols of lithium. Despite this, during the conversion reaction of lithiated  $\text{SnS}_2$ , 4 mols of lithium are consumed in the irreversible formation of  $\text{Li}_2\text{S}$ . As a result, if the irreversible reaction is made reversible, then the theoretical capacity of  $\text{SnS}_2$  could be as high as 1231 mAh/g (8.4 mol  $\text{Li}^+$  per mol  $\text{SnS}_2$ ) [87]. Lithiation causes  $\text{SnS}_2$  to decompose into metallic tin and  $\text{Li}_2\text{S}$  during the first discharge. Tin alloys/dealloys up to the theoretical limit of  $\text{Li}_{4.4}\text{Sn}$ , and  $\text{Li}_2\text{S}$  act as an inert matrix that surrounds the active Sn grains during substantial charge and discharge processes [86]. Li-ions can intercalate to some extent into the  $\text{SnS}_2$  layers without generating phase dissolution, according to earlier publications [45,50]; hence, the reaction can be separated into three phases, as follows in Equations (3)–(5):



To enhance the energy density and capacity of battery materials, a detailed understanding of electrode thermodynamics and chemistry is required [83,84]. First principles have been utilized to study the Li-ion intercalation and diffusion in pristine and modified  $\text{SnS}_2$  interlayers. The data suggest that Li intercalation prefers the octahedral interstitial location. The minimum energy path of Li-ion diffusion in the  $\text{SnS}_2$  interlayer is explored. Researchers have discovered that Li atoms spread from one energetically favorable octahedral interstitial location to the next [63]. The results of this study suggest that regulating the inactive morphologies of  $\text{SnS}_2$ -based anode materials may be a viable strategy for improving their electrochemical performances.

### 3. Pure $\text{SnS}_2$

The  $\text{SnS}_2$  anode material for LIBs was first reported in 1998 by T. Brousse and his team [86].  $\text{SnS}_2$  is an n-type semiconductor “layered compound”, with a hexagonal cadmium iodide ( $\text{CdI}_2$ ) structure that has the potential to own a high capacity [88–92].  $\text{SnS}_2$  can host molecular guest species in vacancies between its neighboring sulfur layers because of its layered structure, similarly to how Li-ion is embedded in graphite [50,66,83,84,93]. For pure  $\text{SnS}_2$  anodes, different structures have been designed and investigated, such as nanoparticles [67,83], nanosheets [50,94–97], nanowalls [98,99], and nanoflowers [100–103], that show different capacities according to their morphologies.

For example, Momma et al. [92] observed that the amorphous  $\text{SnS}_2$  powder could be a viable candidate material for LIBs. An aqueous solution of  $\text{SnCl}_4$  and thioacetamide was sonicated in air at ambient temperature for 30 min to improve crystallinity before being annealed at 400 °C. The cell with the unannealed  $\text{SnS}_2$  electrode had an initial capacity of 300 mAh/g at a current density of 50 mA/g. After annealing, the capacity of  $\text{SnS}_2$  increased to above 600 mAh/g. The results showed that the crystalline morphology of annealed  $\text{SnS}_2$  has been revealed as a possible anode candidate for LIBs because it could accelerate the lithiation process.

Reducing the particle size of Sn-based materials to the nanoscale range is an efficient technique to improve cycling stability. Various methods have been developed for the synthesis of SnS<sub>2</sub> nanostructures with various diameters (from 10 to 100 nm) and morphologies (i.e., nanoparticles, nanorods, nanobelts, nanotubes, and nanosheets) [104–116]. Kim et al. synthesized novel crystalline SnS<sub>2</sub> nanosheets/nanoplates and applied them as anode materials for LIBs [50]. SnS<sub>2</sub> nanosheets from ~1.6 to ~26 nm were successfully prepared via a simple, catalyst-free solvothermal route, without surfactants/functional groups. Ethylene glycol was used as a reducing agent by capping the Sn-ion source, resulting in creating a polymer network and the prevention of nanosheet aggregation. Li-ions could be embedded in the SnS<sub>2</sub> layer to some extent without causing phase decomposition for nanosheet structures.

During the lithiation/delithiation process, many efforts have been undertaken to minimize the volume change and improve cycle performance. Du et al. [97] introduced an *eco*-accommodating and conservative manufacturing method for two-dimensional (2D) layered SnS<sub>2</sub> nanoplates by one-pot synthesis using SnCl<sub>2</sub>·2H<sub>2</sub>O powder (Figure 1a). Figure 2b shows the crystal structure of SnS<sub>2</sub> nanoplates with alternating S-Sn-S layers and S-S layers along the z-axis (c-axis). The final fabricated cell exhibited highly reversible capacity and good capacity retention after 30 cycles (Figure 1c,d). Seo et al. [94] discovered 2D layered nanostructures by thermal decomposition and provided better cyclability due to their unique nanoscale phenomena below 150 nm (Figure 1e,f). The determined average discharge capacity could be up to 583 mAh/g, which was 90% of the maximum theoretical reversible value and 1.6 times the commercial carbon electrode (372 mAh/g), as shown in Figure 1g. This exhibited greatly improved host capabilities as an active LIB electrode because of its unique shape, which consists of a finite, lateral sized, and well-defined layered structure.

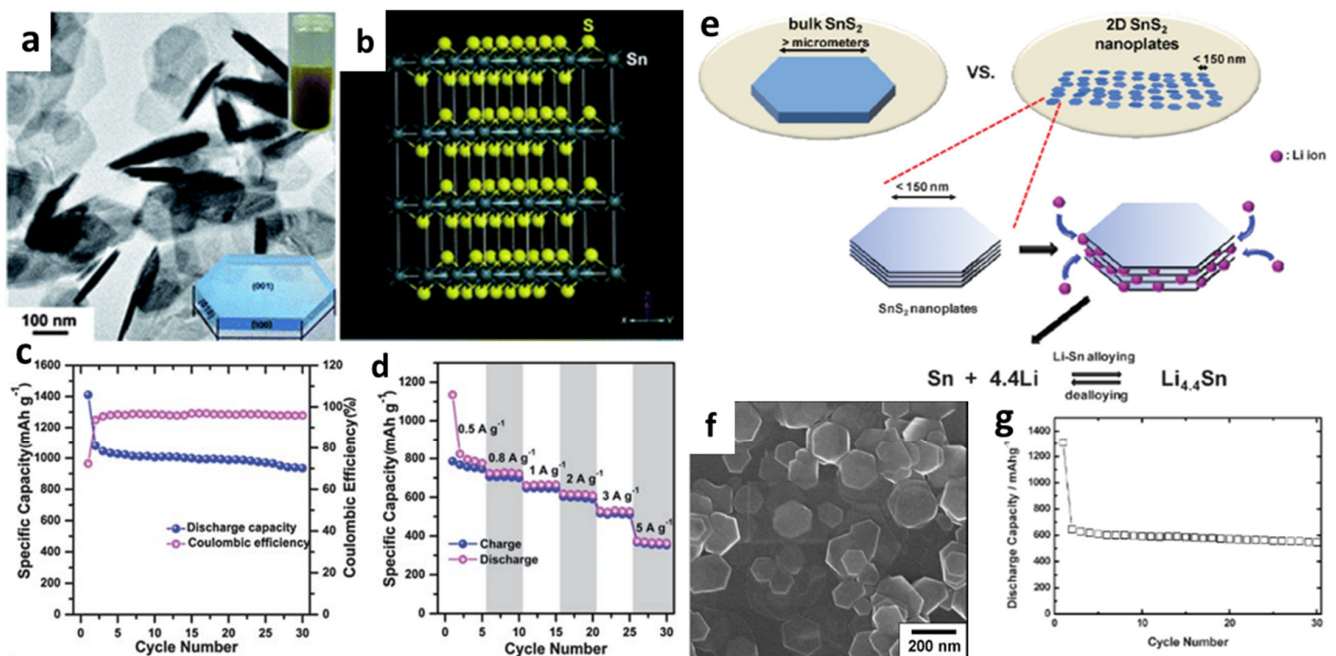


**Figure 1.** (a) A TEM image of hexagonal SnS<sub>2</sub> nanoplates. Inset: (top) photograph of SnS<sub>2</sub> nanoplate solution; (bottom) schematic diagram of a SnS<sub>2</sub> nanoplate. (b) The supercell structure of a SnS<sub>2</sub> crystal with A = 3a, B = 3b, C = 3c. (c) Cycling performance of the SnS<sub>2</sub> nanoplate electrode at a current density of 0.2 A/g and (d) charge-discharge capacities at various current densities from 0.5 to 5 A/g. Reprinted with permission from Ref. [97]. Copyright 2013 RSC. (e) A schematic of lithiation processes for bulk versus nanoplates. (f) An SEM image of SnS<sub>2</sub> nanoplates; (g) life cycle performance of the SnS<sub>2</sub> electrode. Reprinted with permission from Ref. [94]. Copyright 2008 John Wiley and Sons, Inc.

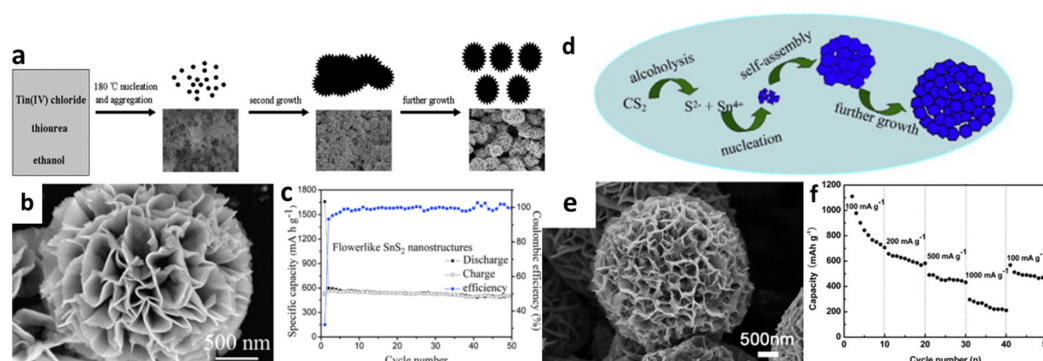


**Figure 2.** (a) Schematic illustration of the morphological evolution process, (b) an SEM image, and (c) cycling performance of the 3D flower-like  $\text{SnS}_2$ . Reprinted with permission from Ref. [66]. Copyright 2010 Elsevier. (d) Schematic illustration of the morphological formation process, (e) an SEM image, and (f) rate capabilities of  $\text{SnS}_2$  hierarchitectures. Reprinted with permission from Ref. [102]. Copyright 2013 Elsevier.

The vertically aligned 2D  $\text{SnS}_2$  nanowalls can also serve as an ideal anode material for LIBs. Liu et al. [98] performed a simple chemical bath deposition method to prepare  $\text{SnS}_2$  nanowall arrays grown directly on copper foils. The shape of these arrays offers numerous benefits for enhancing electrocatalytic activity. Because there are more space between neighboring nanowalls, the electrolyte may readily diffuse into the inner area of the electrode, and the volume change associated with  $\text{Li}^+$  insertion and extraction can be maintained. In the meantime, a simple, biomolecule-assisted technique was used to produce vertically aligned  $\text{SnS}_2$  ultrathin nanosheet arrays on Sn substrate by Zhong et al. [99]. A facile, L-cysteine-assisted hydrothermal strategy was devised to manufacture a graphene-like  $\text{SnS}_2$  film comprising 2–5 atomic layers on Sn foils. The electrochemical discharge capability of the cell with ultrathin  $\text{SnS}_2$  nanosheets was 690 mAh/g at 3C that was near to the theoretical limit.

The formation of 3D flower-like structures was initially proposed early in 2010 by Liu et al. [66]. The electrochemical characteristics of flower-like  $\text{SnS}_2$  systems were remarkable according to the achieved results. These flower-like  $\text{SnS}_2$  structures were prepared by a solvothermal ethanol method and produced nanoplates with thicknesses of about 5–10 nm, which revealed a reversible capacity of about 502 mAh/g after 50 cycles at a current density of 200 mA/g (Figure 2a–c). Wu et al. [102] used  $\text{CS}_2$  for the dissolve in ethanol to form a homogeneous solution, in which  $\text{CS}_2$  acted as a sulfur donor throughout the solvothermal process and  $\text{S}^{2-}$  was released as a source of sulfides (Figure 2d,e). The cell with such prepared electrodes could have capacities of 706.7, 582.4, 432.8, and 210.8 mAh/g, at current densities of 100, 200, 500, and 1000 mA/g, respectively, and it was reversible back to 471 mAh/g when lowering the current density to 100 mA/g (Figure 2f). The overall capacity retained was 73% of the theoretical reversible capacity. The enhanced performance might be because the diffusion distance for ionic and electronic transport was greatly reduced, caused by the specific porous structures of the thin nanosheets, which were accessible for electrolytes and sufficiently dissipated the mechanical stress resulting from the severe volume change during Li-ion uptake/removal. Compared with  $\text{SnS}_2$  nanoparticle anodes, the layered porous structure and flower-like building blocks of these  $\text{SnS}_2$  nanoflowers make the redox reaction and charge transfer kinetics at the electrode faster, and show a much higher discharge capacity than  $\text{SnS}_2$  nanoparticles [116].

Among those morphologies, nanowall- and nanoflower-based  $\text{SnS}_2$  anodes provide more stable cyclic ability. However, within similar morphology, the particle or plate size has a significant impact on the lithiation and delithiation process, depending on the method, reaction time, reaction temperature, annealing, and crystallinity of the material. The electrochemical performance of pure  $\text{SnS}_2$ -based anode is summarized in Table 1. For tin-based electrode materials, an increase in current density usually results in significant capacity

fading. As can be seen, bare SnS<sub>2</sub>-based anode materials continue to be obviously harmed by large initial irreversible capacity losses, severe internal stress, and loss of electrical contact with the current collector. Some primary strategies have been adopted to address these current issues. The initial objective is to create a variety of novel, nanostructured SnS<sub>2</sub> materials, including nanoparticles, nanosheets, and nanoflowers. Not only may nanoscale materials reduce the diffusion length of electrons and lithium ions, but they can also mitigate the large volume impact. However, the nanostructured or porous-structured material alone does not appear to be capable of completely resolving the abovementioned issues, particularly at long cycles and high rates. Thus, using cost-effective carbonaceous materials along with their easy processes is a unique technique which has been considered for increasing the capacity and cycling stability of SnS<sub>2</sub>.

**Table 1.** Electrochemical performance of pure SnS<sub>2</sub>-based anodes with various morphologies.

Materials	Morphology	Size/Thickness (nm)	Initial CE	Specific Capacity (mAh/g)	Rate Performance (mAh/g)	Ref.
SnS <sub>2</sub>	Nanoparticle	N/A	<50%	400/50 mA/g, 25th cycle	N/A	[83]
SnS <sub>2</sub>	Nanoparticle	30	N/A	404/50 mA/g, 30th cycle	N/A	[67]
SnS <sub>2</sub>	Nanosheet	2–26	43%	500/323 mA/g, 50th cycle	~368/3.2 A/g	[50]
SnS <sub>2</sub> (3D)	Microsphere	10	34%	570/650 mA/g, 100th cycle	264/6.5 A/g	[95]
SnS <sub>2</sub> (2D)	Nanoplate	10	36%	521/100 mA/g, 50th cycle	340/3 A/g	[96]
SnS <sub>2</sub> (2D)	Nanoplate	35	73%	935/200 mA/g, 30th cycle	370/5 A/g	[97]
SnS <sub>2</sub> (2D)	Nanoplate	16	~50%	583/323 mA/g, 30th cycle	N/A	[94]
SnS <sub>2</sub> (NW)	Nanowall	<50	36%	700/0.3 C, 40th cycle	400/1.2 C	[98]
SnS <sub>2</sub>	Nanosheet	1–3	~44%	900/1 C, 10th cycle	360/5 C	[99]
SnS <sub>2</sub> (3D)	Nanoflower	5–10	~32%	502/200 mA/g, 50th cycle	N/A	[66]
SnS <sub>2</sub> (3D)	Nanoflower	30	~30%	519/100 mA/g, 50th cycle	297/0.8 A/g	[101]
SnS <sub>2</sub> (3D)	Nanoflower	50	N/A	549/100 mA/g, 100th cycle	210/1 A/g	[102]

#### 4. SnS<sub>2</sub>/Carbon Composites

##### 4.1. Amorphous Carbon/SnS<sub>2</sub> Composites

Amorphous carbon has garnered considerable interest in energy-storage applications due to its high electrochemical activity and inexpensive cost [117–125]. It has been widely shown to improve the capacity and cycling stability of electrodes.

For instance, Kim et al. [121] first discovered carbon-coated SnS<sub>2</sub> nanoparticles, in a study in which SnS<sub>2</sub> powder was extracted from SnCl<sub>4</sub>·5H<sub>2</sub>O and thioacetamide by the solvothermal method and the carbon coating was derived from glucose. After 50 cycles, the C-SnS<sub>2</sub> nanocomposite had a high reversible capacity of 668 mAh/g at a current density of 50 mA/g, superior to bare SnS<sub>2</sub> nanoparticles in terms of cycle performance and rate capability, which owed to the conductive carbon shells and their close association with inert nanoscale SnS<sub>2</sub> materials. Furthermore, a simple, high-energy ball-milling method was developed to synthesize SnS<sub>2</sub>/carbon (SnS<sub>2</sub>/C-x, x = 40, 50, 60 wt.%) nanocomposites in order to study the effect of carbon contents on the overall performance by Zhao et al. [122]. The results indicated that the SnS<sub>2</sub>/C-50 nanocomposite exhibited a remarkably high capacity of 700 mAh/g and stable cycle capacity of 540 mAh/g after 100 cycles at the same current rate of 100 mA/g. SnS<sub>2</sub> NPs were uniformly implanted inside the graphite nanoparticles network after the ball-milling method, which could provide a large number of Li-ion storage sites, excellent electronic conductivity, and rapid ion diffusion, as well as a reduction in SnS<sub>2</sub> volume expansion during cycling. Li et al. [123] prepared a 3D mesoporous carbon anchored with SnS<sub>2</sub> nanosheets (MC-SnS<sub>2</sub> NSs) by sonochemical reflux method with the structural features of both the 2D nanosheet and the 3D porous carbon matrix, which were expected to show improved Li storage efficiency. The composite showed better cyclic performance and improved structural stability compared with the bare-nanoplate-based SnS<sub>2</sub>-C anode. A stable discharge of 428.8 mAh/g at 100 mA/g after 50 cycles with a retention of 64.4% could be achieved by the MC-SnS<sub>2</sub> NSs.

Compared with other regularly utilized carbon sources, different biomass-derived carbons have also been employed with the benefits of low cost and environmental friendliness [124]. An innovative SnS<sub>2</sub>/biochars (SnS<sub>2</sub>/B) composite with a hierarchical structure composed of SnS<sub>2</sub> nanosheet arrays and biochars carbonized from chewed sugarcane was effectively generated using a simple one-step hydrothermal method [125]. The constructed cell with SnS<sub>2</sub>/B could deliver a high initial discharge specific capacity of 1107.4 mAh/g at 100 mA/g with a CE of 54.8%. Zhang et al. [56] fabricated carbon-encapsulated flower-like SnS<sub>2</sub> nanoplates with (101) plane orientation by a hydrothermal method, with polyethylene glycol (PEG 400) as a surfactant (Figure 3a–c). The SnS<sub>2</sub> nanoplates synthesized without PEG mainly grew along the (001) plane. The cell with the prepared material showed an excellent capability of 796 mAh/g at a current density of up to 2 A/g along with exceptional cycle stability. The cycle attenuation rate of the cell tested at 0.5 A/g for 300 cycles was only 0.05% (Figure 3e). The outstanding results might be ascribed to the use of highly (101) faceted preferred orientation in the design of the microstructures, creating a quick and long-lasting highway for Li-ion diffusion, resulting in rapid reaction kinetics (Figure 3d). Using a hydrothermal synthesis process coupled with membrane technology, flower-like SnS<sub>2</sub> nanosheets, evenly fixed in the pores of the carbon membrane (SnS<sub>2</sub>-CM), were produced by Liu et al. [69]. The unique design proved that membrane technology supplied an abundant membrane pore space for uniform SnS<sub>2</sub> nanosheet development via a C-S covalent connection. For LIBs at 50 mA/g, the highest reversible capacitance could be up to 808.9 mAh/g, which was because thin SnS<sub>2</sub> nanosheets emerged in the membrane hole and surface, enabling the SnS<sub>2</sub> cm a 3D interpenetrating network of porous morphology. The novel 3D porous structure not only assisted fast ion transit channels and lowered diffusion length, but also provided ample void space for SnS<sub>2</sub> nanosheet volume growth during long-term cycles. The C-S covalent bond also maintained a close contact between SnS<sub>2</sub> and the carbon membrane, contributing to structural stability.

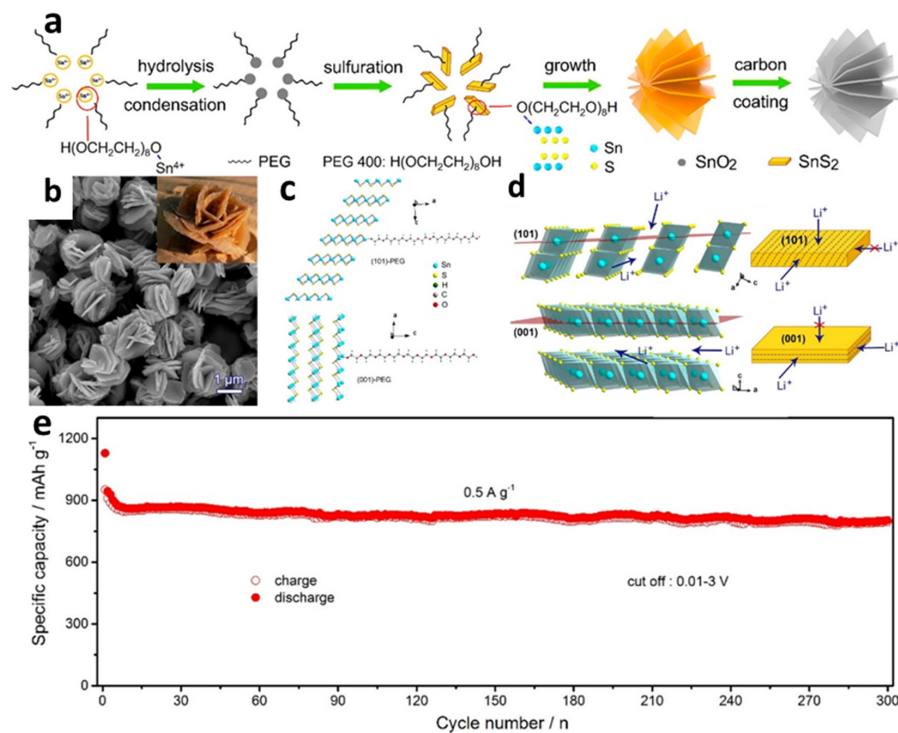


**Figure 3.** (a) Schematic illustration of the formation process; (b) SEM images of carbon-encapsulated SnS<sub>2</sub> nanoplates; (c) structural models of terminated (101) and (001) surfaces of SnS<sub>2</sub> with adsorbed PEG for first-principles calculation; (d) schematic illustration of Li-ion insertion; (e) long-term cycling performance of carbon-encapsulated SnS<sub>2</sub> nanoplates with the (101)-oriented plane. Reprinted with permission from Ref. [56]. Copyright 2017 ACS.

However, SnS<sub>2</sub> with amorphous carbon typically has a low reversible capacity. Besides, a better rate capability is desirable for next-generation LIBs. Thus, alternative carbon-based materials, such as carbon nanotubes (CNTs) and graphene, are being investigated in combination with SnS<sub>2</sub> in order to increase their specific capacity and rate capability, and also resolve the issues related to pure SnS<sub>2</sub>-based anodes.

#### 4.2. CNTs/SnS<sub>2</sub> Composites

SnS<sub>2</sub> combined with CNTs is another way to overcome the shortcomings associated with bare SnS<sub>2</sub> anodes. CNT-based materials may be beneficial for charge transfer and electrode stability, improving the electrochemical performance [126–135].

Zhai et al. [126] first reported SnS<sub>2</sub> nanosheets on multiwall CNTs (MWCNTs) by chemical vapor deposition with a tube diameter around 80–90 nm. SnS<sub>2</sub> nanosheets and nanoflakes were uniformly anchored on CNTs to form SnS<sub>2</sub>/CNT composite anodes with SnS<sub>2</sub> sheaths of different thicknesses, which exhibited higher Li storage capacity and better cycle performance compared with pure SnS<sub>2</sub> (Figure 4a–d). Sun et al. [133] also synthesized SnS<sub>2</sub> nanoflakes decorated on a MWCNT structure through a simple solution-phase method. The cell with the SnS<sub>2</sub>/MWCNTs composite demonstrated initial discharge and charge capacities of 1416 and 518 mAh/g, respectively, and could maintain a reversible capacity of 510 mAh/g after 50 cycles at a current density of 100 mA/g. The improved performance might be attributed to the morphological properties of SnS<sub>2</sub> flakes and the inclusion of MWCNT, that could reduce volume change throughout the cycle, offer more active sites to accept Li<sup>+</sup>, and accelerate the conductivity of the active material. Differently from the above fabricating processes, a SnS<sub>2</sub>/CNTs composite was also produced via a hydrothermal process by in situ vulcanization of SnO<sub>2</sub>/CNTs by Cheng et al. [48]. In the prefabricated SnO<sub>2</sub>/CNTs composite, SnO<sub>2</sub> nanoparticles with diameters less than 5 nm were completely coated on the CNTs via Sn-O-C bonding. SnO<sub>2</sub> nanoparticles were converted into SnS<sub>2</sub> hexagonal nanosheets during the in situ sulphuration reaction, and the Sn-O-C bonding was replaced by C-S bonding. The cell with the obtained SnS<sub>2</sub>/CNTs exhibited superior electrochemical performance, which could deliver an initial reversible capacity of 1202 mAh/g and a capacity of around 660 mAh/g after 100 cycles at 100 mA/g (Figure 4e–g).

In addition, polypyrrole, which is a one kind of carbonaceous substance, is a prospective additive for improving the electrochemical performances of LIBs due to its ease of synthesis, low cost, strong electron conductivity, and environmental stability. Polypyrrole works as a matrix to support the internal stress of electrodes that experience extreme volume changes, as well as providing a conducting backbone for the active materials [135]. Chen et al. [127] prepared composites with a higher initial CE by combining polymerization and hydrothermal process (Figure 5a,b). Two-dimensional SnS<sub>2</sub> nanosheets were used to adorn carbonaceous polypyrrole nanotubes with the interweaving twisted SnS<sub>2</sub> nanosheets, reducing volume change during electrochemical cycling and providing more active sites to react with Li-ions. Figure 5c shows that the initial discharge capacity of carbon polypyrrole nanotubes (CPN)-coated SnS<sub>2</sub> nanosheets was 1422 mAh/g at a current density of 60 mA/g, with a reversible capacity of 699.2 mAh/g after 100 cycles. The excellent electrochemical performance of CPN@SnS<sub>2</sub> composite anode material derived from a unique structure was due to the insertion of conductive CPN, that substantially enhanced the electronic conductivity of the whole anode, allowing for fast electron transmission, as depicted in Figure 5d.

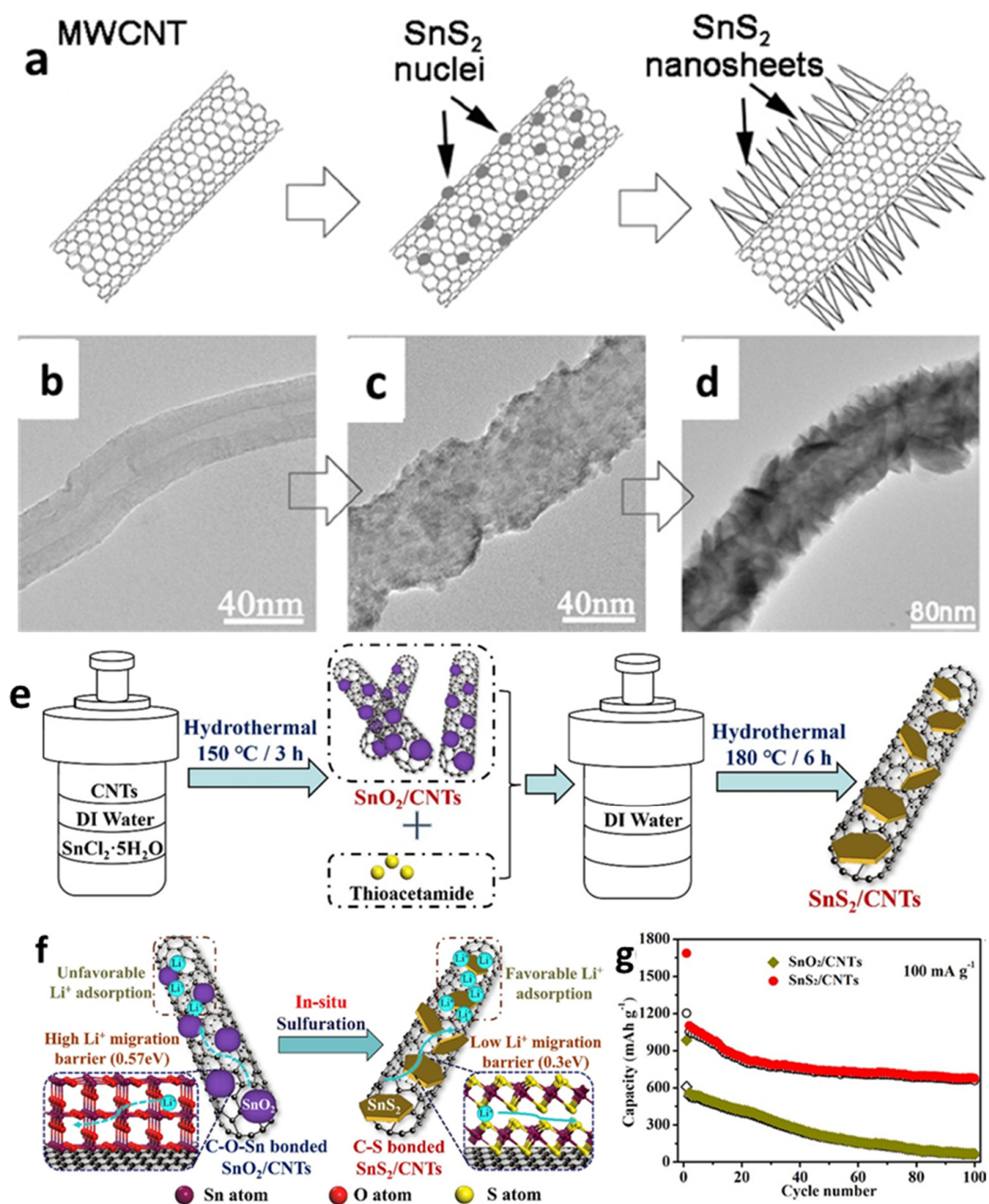


**Figure 4.** (a) Schematic illustration for the growth process of the SnS<sub>2</sub> NS@MWCNTs and (b–d) their TEM images. Reprinted with permission from Ref. [126]. Copyright 2011 ACS. (e) The synthesis procedures diagram; (f) illustration of the Li storage advantage; (g) cycling performance of the SnS<sub>2</sub>/CNTs composite. Reprinted with permission from Ref. [48]. Copyright 2021 Elsevier.

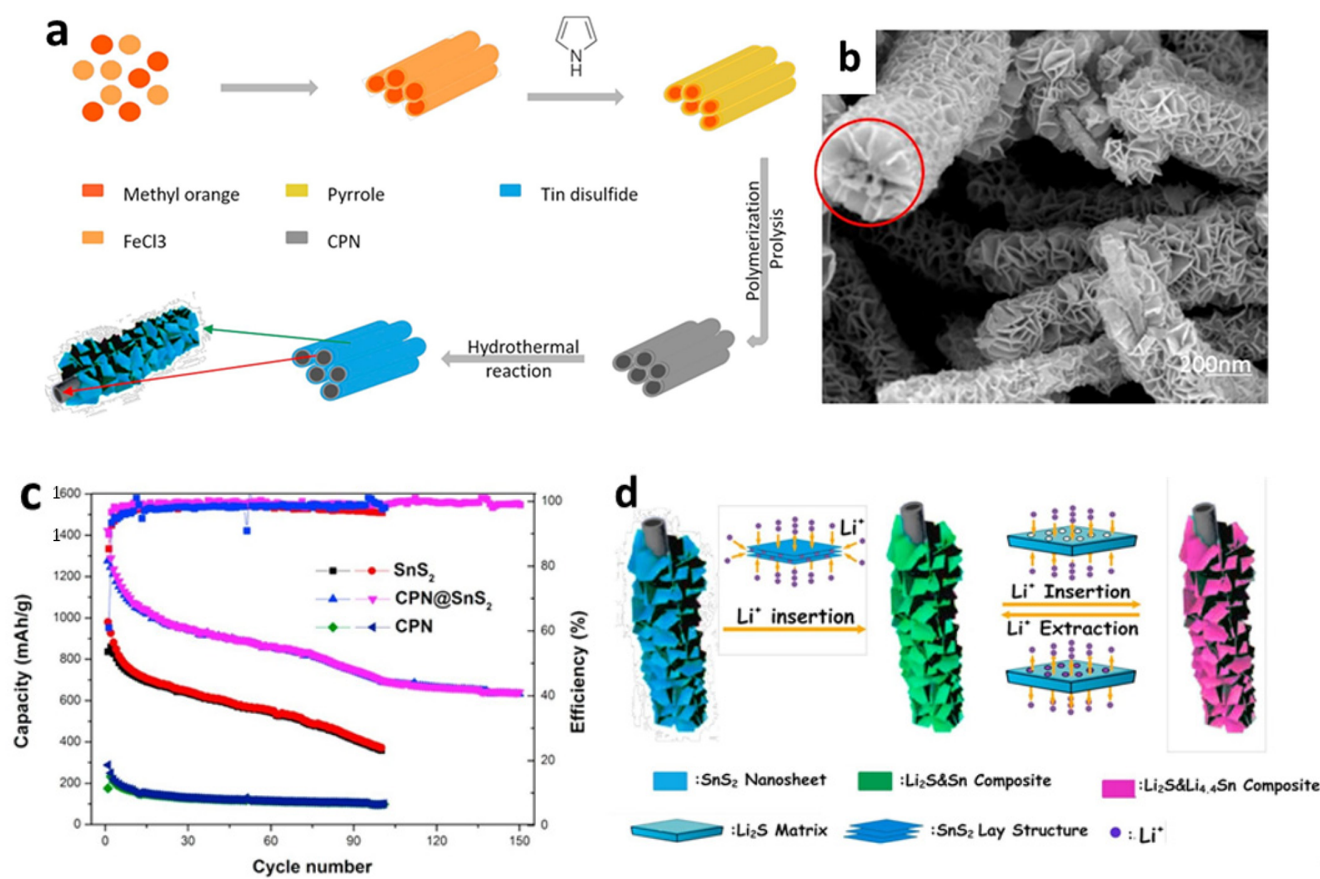


**Figure 5.** (a) Formation mechanism, (b) an SEM image, (c) cycling performance, and (d) a schematic illustration of the Li insertion/extraction mechanism of CPN@SnS<sub>2</sub> composites. Reprinted with permission from Ref. [127]. Copyright 2017 Elsevier.

The electrochemical performance of SnS<sub>2</sub>-CNT-based anodes has been widely explored, and their corresponding results are summarized in Table 2. In order to improve the conductivity of SnS<sub>2</sub>-based materials, it is believed that the combination of electronically conductive agents, such as CNTs, is an effective strategy. An additional effective route is through the morphology-controlled SnS<sub>2</sub>-CNT synthesis of nanostructured, active materials, such as nanowire, nanotubes, nanoflakes, and nanosheets. These nanostructures can shorten the pathway lengths of Li<sup>+</sup> and compensate for volume change due to their large surface-to-volume ratio, which makes them ideal for use in LIBs. Additionally, SnS<sub>2</sub>-graphene-based composites are currently used for further improving electrochemical performance because they allow enormous concentrations of Li<sup>+</sup> to adsorb and desorb during charging and discharging cycles.

**Table 2.** Electrochemical performance of carbon-coated SnS<sub>2</sub> and SnS<sub>2</sub>-CNT-based anodes.

Materials	Morphology	Size/Thickness nm	Initial CE	Specific Capacity (mAh/g)	Rate Performance (mAh/g)	Ref.
C-SnS <sub>2</sub>	Nanoparticle	80	41%	668/50 mA/g, 50th cycle	600/645 mA/g	[121]
SnS <sub>2</sub> /C-x	Nanoparticle	60	80.8%	540/100 mA/g, 100th cycle	300/2 A/g	[122]
MC-SnS <sub>2</sub> NS	Nanoplate	5–15	N/A	428.8/100 mA/g, 50th cycle	150/1 A/g	[123]
C-SnS <sub>2</sub>	Nanoplate	75	78%	800/500 mA/g, 300th cycle	796/2 A/g	[56]
SnS <sub>2</sub> @MWCNT	Nanosheet	80–100	37.2%	420/100 mA/g, 50th cycle	310/500 mA/g	[126]
SnS <sub>2</sub> @MWCNT	Nanoflake	N/A	37%	510/100 mA/g, 50th cycle	329/500 mA/g	[133]
CPN@SnS <sub>2</sub>	Nanosheet	N/A	89.8%	699.2/60 mA/g, 100th cycle	553.5/1.5 A/g	[127]

### 4.3. Graphene/SnS<sub>2</sub> Composites

Graphene is a novel, 2D, “aromatic” single molecule with high electron mobility, a unique electrical structure, high thermal conductivity, mechanical strength, and a large surface area, which has attracted unprecedented attention [136–167]. Many studies have been conducted to design novel SnS<sub>2</sub>/graphene anode materials for LIBs with different nanostructures to improve the electrochemical properties, including nanoparticles/nanocrystals [53,54,137,142,156,158,161,163], nanosheets/nanoplates [141,143,144,150–153], and nanoflowers [49].

For instance, Yin et al. [138] decorated SnS<sub>2</sub> nanocrystals on a reduced graphene oxide (RGO) sheet through the combination of hydrothermal and reduction methods (Figure 6a,b). The cell with the obtained composites showed better cyclic performance with a reversible capacity of 820 mAh/g at a current rate of 0.2 C after 30 cycles compared with a pure SnS<sub>2</sub> anode (Figure 6a–c). Controlling the particle size of electrode materials has been acknowledged as an effective approach for improving the cycle stability and rate characteristics of LIBs [67]. Thus, a simple, one-step hydrothermal process for fabricating composites containing size-tunable tin disulfide on SnS<sub>2</sub>-RGO (Figure 6d–f) was investigated by Zhao et al. to thoroughly explore the effect of particle size on the electrochemical properties of the material [161]. To demonstrate the morphological, size-dependent properties, the particle sizes of SnS<sub>2</sub> nanoparticles were changed by varying the length of the hydrothermal process with three different heat-treatment times (12, 24, or 48 h). The collected samples were marked as SnS<sub>2</sub>/RGO-12, SnS<sub>2</sub>/RGO-24, and SnS<sub>2</sub>/RGO-48, respectively. After 12 h of hydrothermal treatment, the ultrafine SnS<sub>2</sub> particles (12 nm) were evenly spread over the graphene nanosheets. It is seen from Figure 6g that, after 200 cycles at 0.1 A/g, a high reversible capacity of 1211 mAh/g remained, which was because the prepared samples had more active sites and increased transport kinetics, thus yielding significant enhancement in electrochemical performance. Mei et al. [156] reported ultrasmall SnS<sub>2</sub> nanocrystals decorated on flexible RGO through a refluxing method. The supplied composite with a high surface-to-volume ratio could enhance Li atom absorption on both sides of the sheet and porous architectures, enabling the RGO nanosheet to offer enough room for Li<sup>+</sup> storage. The cell with such materials exhibited good capacity retention even at high rates of 1 C and 5 C with the capacities of 773 mA h/g and 415 mAh/g, respectively, after 450 cycles, which were significantly better than the previous hydrothermal-based studies. SnS<sub>2</sub>@RGO nanocomposites were also created using a novel ionic-liquid-assisted method, which employed SnS<sub>x</sub> precursors by reacting elemental tin and sulfur in the ionic liquid, 1-butyl-2, 3-dimethylimidazolium chloride (Figure 6h,i) [163]. Exceptionally high reversible capacity and cycle stability could be achieved by using the obtained composite. A discharge-specific capacity reached 1045.8 mAh/g, even after 700 cycles at a current density of 500 mA/g, as shown in Figure 6j. The improved reversible capacity of the SnS<sub>2</sub>@RGO electrode was explained by electrolyte breakdown at the low potential to create an organic polymeric/gel-like layer due to the “pseudo-capacitance-type behavior” that activated the active material under deep cycling.

Furthermore, a homogeneous layer of SnS<sub>2</sub> nanoparticles was grown on graphene nanosheets (SnS<sub>2</sub>@GNS) and linked by covalent bonds using the solvothermal method (Figure 7a–c) [162]. The I<sub>D</sub>/I<sub>G</sub> values of SnS<sub>2</sub>@GNS and GNS were calculated to be 1.44 and 1.22, respectively, showing that SnS<sub>2</sub>@GNS had more flaws. High-level flaws in graphene can accelerate ion and electron migration, improve electrochemical reaction kinetics, and offer more active sites for Li-ion adsorption and intercalation [146]. As displayed in Figure 7d, the cell with SnS<sub>2</sub>@GNS delivered a capacity of 1250.8 mAh/g after 150 cycles at 0.1 A/g. In addition, Li et al. [166] prepared SnS<sub>2</sub> nanocrystals (NCs) through the one-pot solvothermal method using carbon shells attached to RGO by C-S covalent bonding (Figure 7e). The well-controlled carbon shells offered long-term protection for SnS<sub>2</sub> NCs against electrolyte corrosion and structural pulverization. Carbon shells could act as mediums, enhancing C-structural SnS<sub>2</sub>@RGO's stability and conductivity. It

is demonstrated that LIBs had superior rate capabilities and cycling stability (capacity retention of 74.7% after 1000 cycles at 2.0 A/g, as shown in Figure 7f).

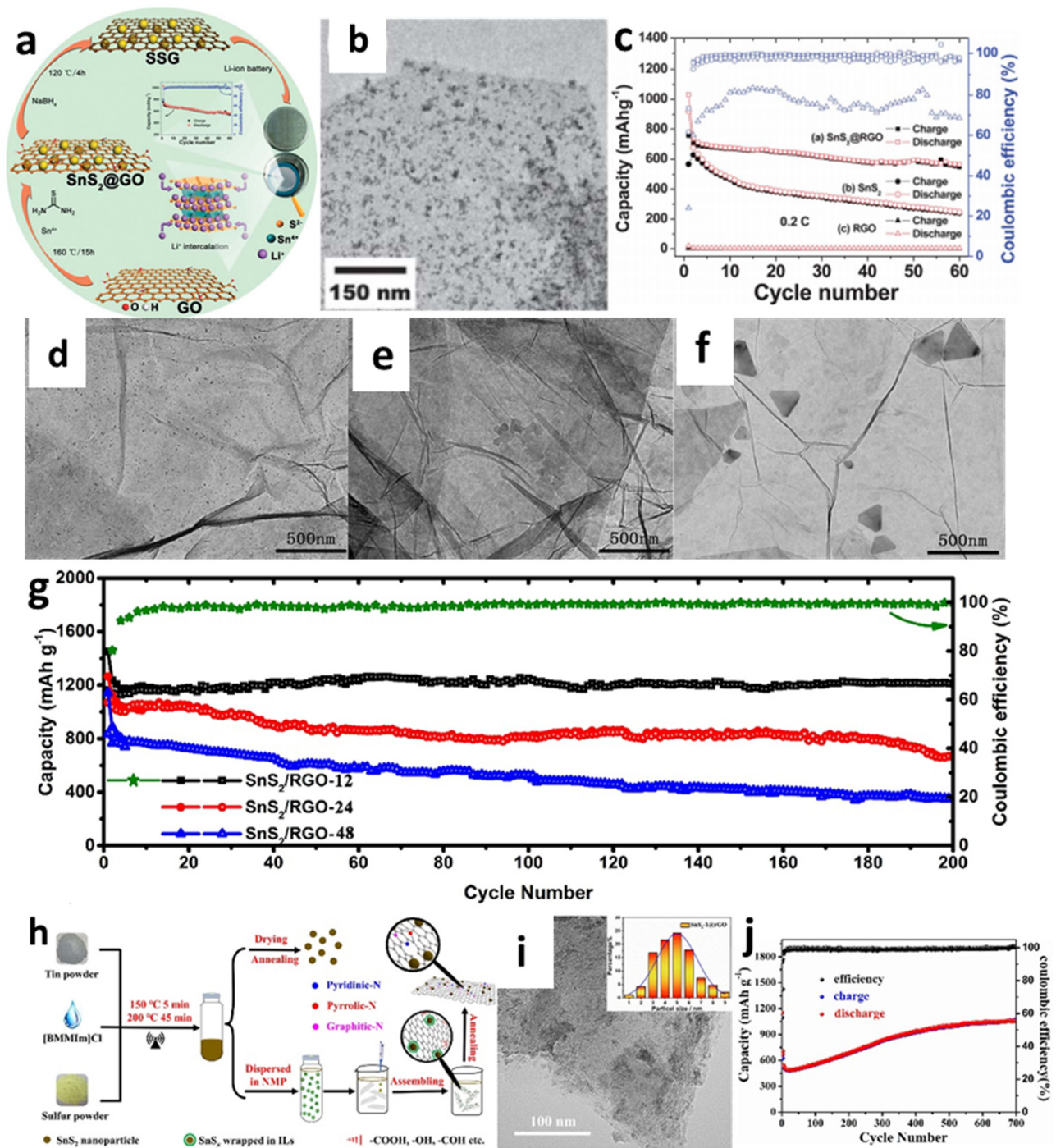


**Figure 6.** (a) Synthetic process, (b) a TEM image, (c) cycling performance of SnS<sub>2</sub>@RGO composite. Reprinted with permission from Ref. [138]. Copyright 2012 RSC. TEM images of (d) SnS<sub>2</sub>/RGO-12, (e) SnS<sub>2</sub>/RGO-24, and (f) SnS<sub>2</sub>/RGO-48; (g) cycling performance of SnS<sub>2</sub>/RGO. Reprinted with permission from Ref. [161]. Copyright 2020 Elsevier. (h) Schematic illustration of the synthesis, (i) a TEM image, and (j) cycling performance at a current density of 500 mA/g of SnS<sub>2</sub>@RGO. Reprinted with permission from Ref. [163]. Copyright 2021 Elsevier.

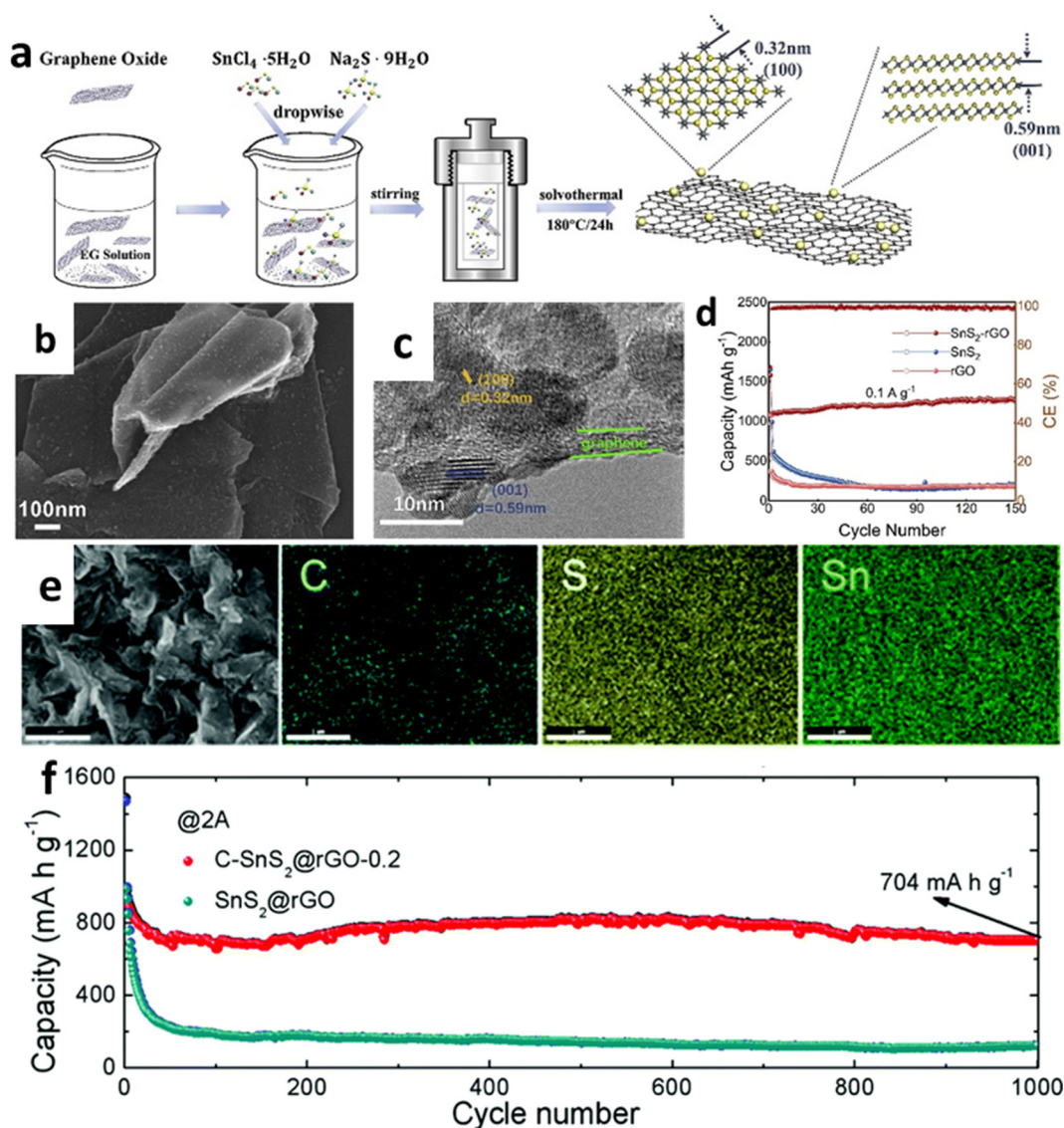


**Figure 7.** (a) Synthesis procedures diagram, (b) TEM and (c) HRTEM images, and (d) cycling performance of SnS<sub>2</sub>@GNS. Reprinted with permission from Ref. [162]. Copyright 2020 Elsevier. (e) An SEM image and EDX mapping of C, S, and Sn elements; (f) long-term cycle stability of C-SnS<sub>2</sub>@RGO. Reprinted with permission from Ref. [166]. Copyright 2020 RSC.

Moreover, Luo et al. [142] developed a new porous nanostructure composed of 2D graphene–SnS<sub>2</sub> (G-SnS<sub>2</sub>) by transforming SnO<sub>2</sub> nanoparticles into 2D SnS<sub>2</sub> nanoplates directly on/between graphene nanosheets via a solution approach followed with a chemical vapor deposition (CVD) process (Figure 8a,b). The cycling performance in Figure 8c showed that the cell with the prepared G-SnS<sub>2</sub> had a stable capacity of 650 mAh/g after 30 cycles at 50 mA/g, while the reversible capacity of bare SnS<sub>2</sub> gradually decreased to 277 mAh/g. Xia et al. [146] synthesized pristine SnS<sub>2</sub> nanosheets with a thickness of 5 nm by a hydrothermal process, and then uniformly layered SnS<sub>2</sub> on graphene sheets to produce layer-by-layer nanosheets (LL-SnS<sub>2</sub>/G) through the ball-milling method (Figure 8d,e). When used as anodes for LIBs, the capacity reached 1152.25 mAh/g after 100 cycles at a current rate of 100 mA/g, as shown in Figure 8f. The excellent electrochemical performance was attributed to the synergistic effect between SnS<sub>2</sub> nanoplates with high specific capacity and conductivity of graphene, which buffered the volume change and provided an effective physical barrier between the active materials and the electrolyte to suppress the shuttle effect of polysulfides formed during delithiation processes. Chen et al. [157] used reflux

condensation and hydrothermal methods to grow  $\text{SnS}_2$  nanoplates on the surface of RGO nanosheets. When the GO concentration was 15%, the  $\text{SnS}_2/\text{RGO}$  electrode exhibited the excellent electrochemical performance, which showed capacities of 776, 715, 635.6, 595.2, 517.5, and 447.1 mAh/g at current densities of 0.2, 0.5, 1, 2, 5, and 8 C, respectively. In addition, 3D nanoplate-based  $\text{SnS}_2/\text{graphene}$  was synthesized through a facial solvothermal method by Zhang et al. [151], in which  $\text{SnS}_2$  nanoplates with an average thickness of 3.6 nm were well dispersed and tightly contacted onto graphene substrates (Figure 8g,h). The cell with  $\text{SnS}_2\text{-G}$  achieved a very stable capacity of 826 mAh/g over 200 cycles at 500 mA/g. The specific capacities of 854, 780, 728, 625, and 498 mAh/g were obtained under the conditions of 0.5, 1, 2, 4, and 8 A/g, respectively (Figure 8i,j). The enhanced electrochemical performance of the cell was because of the enormous surface area of 2D hybrid materials, the highly conductive and flexible graphene matrix, the 3D design, the facilitated electrolyte filtration, and the smooth ion transport.

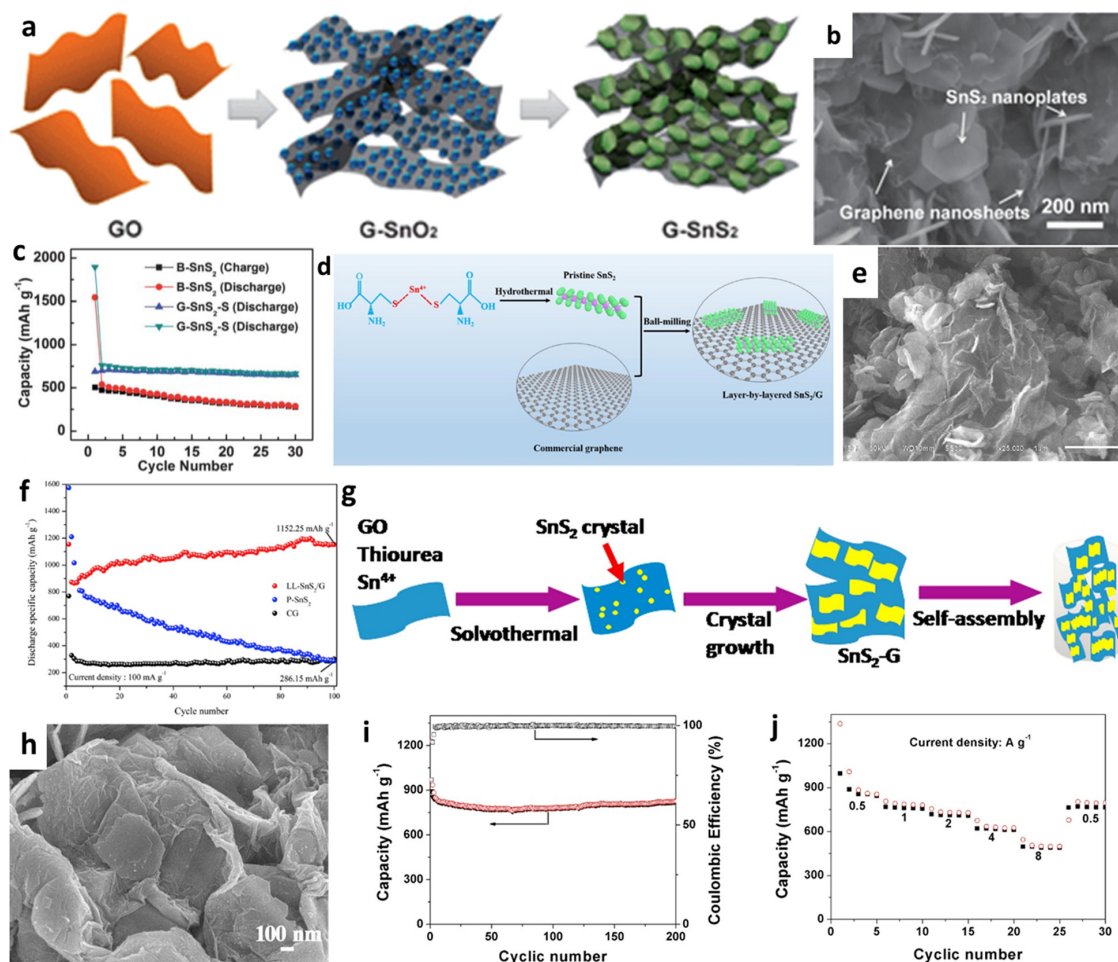


**Figure 8.** (a) Illustration of the formation, (b) an SEM image, and (c) cycling performance of the  $\text{G-SnS}_2$ . Reprinted with permission from Ref. [142]. Copyright 2012 RSC. (d) Schematic illustration of the formation, (e) an SEM image, and (f) cycling performance of  $\text{LL-SnS}_2/\text{G}$ . Reprinted with permission from Ref. [146]. Copyright 2018 Elsevier. (g) Schematic formation, (h) an SEM image, (i) cycling performance, and (j) rate capability of  $\text{SnS}_2\text{-G}$ . Reprinted with permission from Ref. [151]. Copyright 2016 Elsevier.

Meanwhile, due to the high porosity, low density, and large pore volume, several self-assembled graphene aerogels (GAs) and composites of 3D graphene-embedded metal or metal oxide nanoparticles have been successfully manufactured using various approaches [150–152,168–170]. For instance, Tang et al. [148] prepared a unique 3D

SnS<sub>2</sub>/graphene (SSG) composite through transforming SnO<sub>2</sub> nanoparticles anchored on GO sheets directly into SnS<sub>2</sub> nanoplates, homogeneously embedded in the graphene frameworks (Figure 9a,b). The diameter of the obtained nanoplates on graphene was about 300 nm. The initial discharge and charge capacities of the cell were 1677 and 1159 mAh/g, respectively. A reversible capacity of 1060 mAh/g was retained after 200 cycles at a current density of 100 mA/g. When the current density declined from 2000 to 100 mA/g, it was found that the reversible capacity could be up to 1100 mAh/g (Figure 9c,d). Jiang et al. [150] successfully fabricated 3D SnS<sub>2</sub>/graphene aerogels (SnS<sub>2</sub>/GAs) via an in situ hydrothermal method for self-assembly of graphene sheets followed by freeze-drying to maintain a stable 3D structure (Figure 9e). Figure 9f illustrates that the cell with SnS<sub>2</sub>/GAs exhibited high-rate capability and cycling stability, which could be ascribed to the unique 3D interconnected architectures of the aerogels and the synergistic effects of the layered SnS<sub>2</sub> and the graphene, providing enough sites for absorbing Li-ions and shortening transport distance between electrode and electrolyte. Additionally, 3D sandwich-like SnS<sub>2</sub>/graphene/SnS<sub>2</sub> with expanded interlayer distance was introduced by Jiang et al. [149]. The covalently SnS<sub>2</sub> nanosheets were decorated on both sides of RGO sheets to form an SnS<sub>2</sub>/RGO/SnS<sub>2</sub> anode composite. The presence of GO could provide a nucleation site for SnS<sub>2</sub> and promote SnS<sub>2</sub> nanoplates aggregate and grow to form fewer layers. SnS<sub>2</sub> nanosheets were chemically linked to graphene through the C-S bonds to produce a sandwich structure with specific capacities of 844 mAh/g after 200 cycles at a current density of 1 A/g (Figure 9g–i).

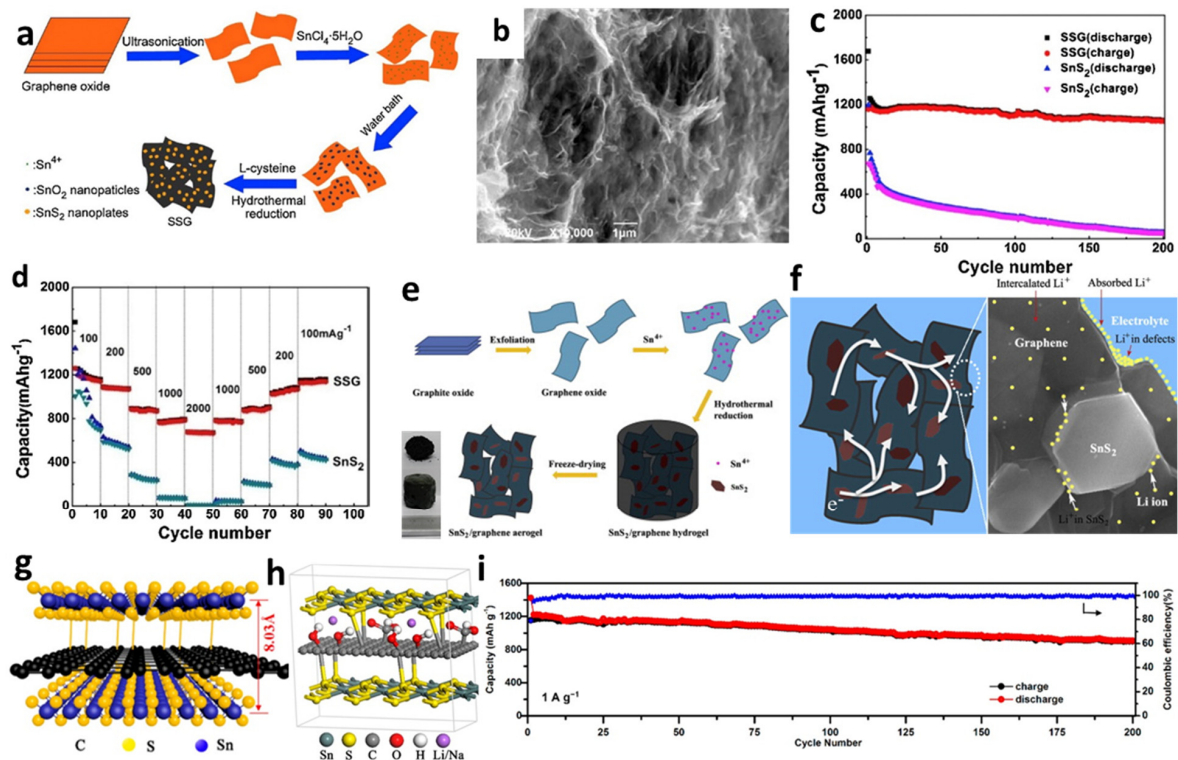


**Figure 9.** (a) Schematic formation process, (b) an SEM image, (c) cycling performance, and (d) rate capability of SSG. Reprinted with permission from Ref. [148]. Copyright 2015 Elsevier. (e) Fabrication process, and (f) schematic representation of electron transmission and lithium ions storage of SnS<sub>2</sub>/GAs. Reprinted with permission from Ref. [150]. Copyright 2013 Elsevier. (g) Schematic illustration, (h) molecular model, and (i) high rate cycling performance of SnS<sub>2</sub>/RGO/SnS<sub>2</sub>. Reprinted with permission from Ref. [149]. Copyright 2019 ACS.

Apart from nanosheets, Ren et al. [144] introduced SnS<sub>2</sub> nanoflakes on the 3D graphene foams (GFs) using a single-mode microwave hydrothermal technique (Figure 10a,b). The composite SnS<sub>2</sub>@GF electrode provided a high capacity of 818.4 mAh/g at a high current

density of 1.0 A/g after 500 cycles, as seen from Figure 10c. The GF served as a 3D framework for SnS<sub>2</sub> nanoflakes loading and this conductive porous matrix was convenient for rapid electron transport, reduced the strain during the intercalation/extraction process, and provided a large electrode/electrolyte contact area. A new nanocable-like structured SnS<sub>2</sub>-graphene network was fabricated by Kong et al. [158], in which graphene layers were rolled up to embody SnS<sub>2</sub> nanosheets with a thickness of around 10 nm. SnS<sub>2</sub>@G nanocable showed the initial discharge and charge capacities of 1334 and 764 mAh/g, respectively (Figure 10d–f). Figure 10g presents that the composite maintained the reversible capacity of 720 mAh/g at 200 mA/g up to 350 cycles with over 93.5% capacity retention. This might be attributed to the unique structure design which released the volume change of SnS<sub>2</sub> during discharge–charge cycles and promoted easy access of electrolytes to dynamic anode materials. Liu et al. [49] synthesized nanoflower-based SnS<sub>2</sub>@RGO (SnS<sub>2</sub>-NF@RGO) composite anodes for LIBs (Figure 10h). The initial specific capacities of SnS<sub>2</sub>-NS and SnS<sub>2</sub>-NF were 1300 and 1100 mAh/g, respectively, and gradually decreased to below 200 mAh/g after 200 cycles under 615.5 mA/g, while SnS<sub>2</sub>-NF@RGO maintained reversible capacity of 525 mAh/g after 360 cycles and capacities of 1211.8, 1021.7, 809.1, 708.1, 412.5, 509.6, 751.5, 820.3, and 923.5 mAh/g under 123.1, 246.2, 615.5, 1231, 2462, 1231, 615.5, 246.2, and 123.1 mA/g, respectively (Figure 10i,j). It revealed good capacity retention through the layer structure of RGO additives, which gave better conductivity between SnS<sub>2</sub>-NF/electrolyte interfaces and minimized the self-aggregation during the Li<sup>+</sup> insertion/deinsertion processes.

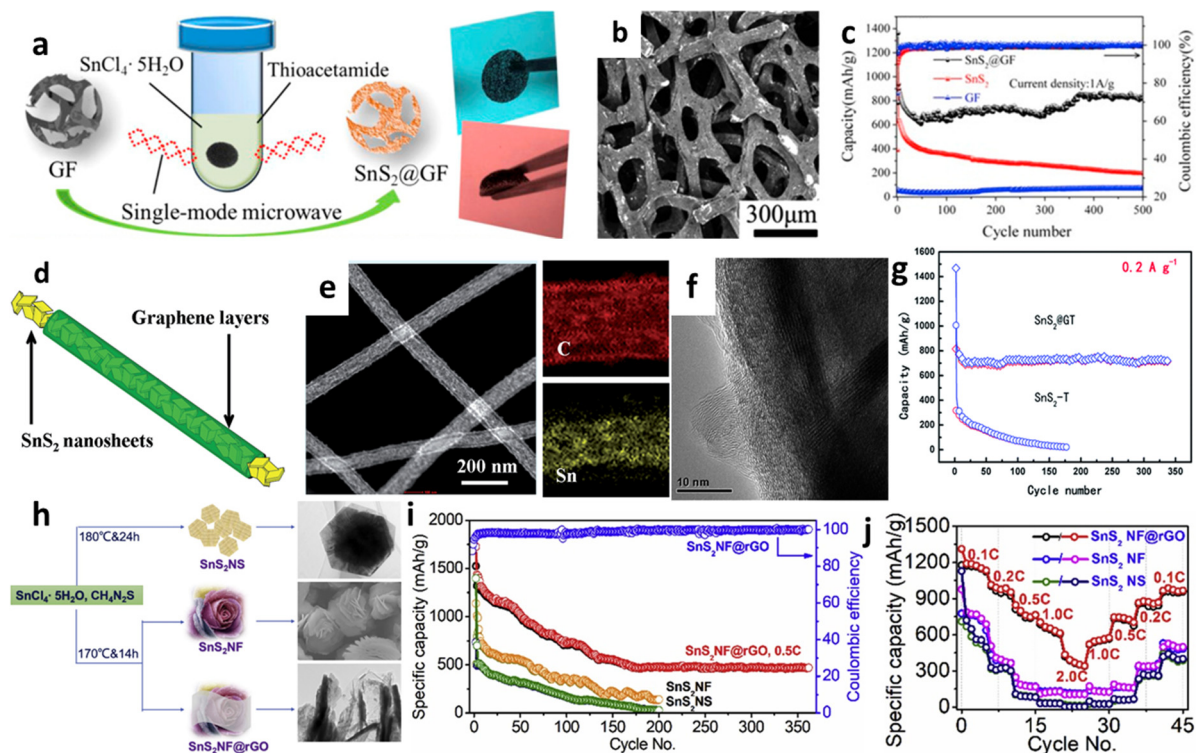


**Figure 10.** (a) Schematic illustration of the formation, (b) an SEM image, and (c) cycling performance of SnS<sub>2</sub>@GF. Reprinted with permission from Ref. [144]. Copyright 2016 Elsevier. (d) Schematic illustration, (e) an SEM image and mapping, (f) a TEM image, and (g) cycling performance of SnS<sub>2</sub>@G. Reprinted with permission from Ref. [158]. Copyright 2014 RSC. (h) Schematic diagram and SEM images, (i) cycling performance, and (j) rate capability of SnS<sub>2</sub>-NF@RGO. Reprinted with permission from Ref. [49]. Copyright 2019 Elsevier.

The electrochemical performance of SnS<sub>2</sub>/graphene anodes is summarized in Table 3. It can be seen that SnS<sub>2</sub>/graphene-based anodes have attracted great attention thanks to the synergistic interaction of SnS<sub>2</sub> and graphene. On one hand, the graphene sheets could

not only prevent the aggregation of microscopic SnS<sub>2</sub>, but also significantly improve the electrode's electronic conductivity and buffer volume changes during charge/discharge processes. The inclusion of SnS<sub>2</sub> between graphene sheets, on the other hand, could successfully prevent graphene restacking. In recent years, a variety of methods have been utilized to make SnS<sub>2</sub>-G nanocomposites, each with its own set of benefits. For example, by simply altering the reaction conditions and additives, hydrothermal/solvothermal methods and other solution-based methods are most typically employed to create SnS<sub>2</sub>/graphene nanocomposites with various nanostructures. SnS<sub>2</sub> nanostructures, such as nanoparticles, nanorods/nanowire, 2D nanosheets/films, and 3D nanoflowers, can reduce volume change during charge/discharge and can shorten the diffusion length of Li-ions, which is critical for boosting cells' rate capability and cycle stability.

**Table 3.** Electrochemical performance of SnS<sub>2</sub>/graphene-based anodes.

Materials	Morphology	Size/Thickness nm	Initial CE	Specific Capacity (mAh/g)	Rate Performance (mAh/g)	Ref.
G/SnS <sub>2</sub>	Nanoparticle	30	29.6%	351/200 mA/g, 50th cycle	N/A	[54]
RGO-SnS <sub>2</sub>	Nanoparticle	100	63.44%	405/0.5 C, 80th cycle	200/5 C	[53]
SnS <sub>x</sub> -G, 1 < x < 2	Nanoparticle	5	69%	860/0.2 C, 150th cycle	450/2 C	[137]
SnS <sub>2</sub> /graphene	Nanocrystal	3–5	71.5%	564/0.2 C, 60th cycle	242/5 C	[138]
SnS <sub>2</sub> -graphene	Nanoparticle	5–20	63.2%	903/200 mA/g, 50th cycle	500/1.6 A/g	[143]
SnS <sub>2</sub> /GNS	Nanoparticle	2–3	~69.9%	577/59.1 mA/g, 50th cycle	200/591 mA/g	[147]
SnS <sub>2</sub> /RGO	Nanocrystal	10–40	35%	644/500 mA/g, 50th cycle	430/1 A/g	[154]
SnS <sub>2</sub> /RGO	Nanocrystal	3–4	78.7%	1034/0.1C, 200th cycle	415/5 C	[156]
SnS <sub>2</sub> NP/GNs	Nanoparticle	4	49%	631.4/100 mA/g, 150th cycle	378/20 A/g	[140]
RGO/SnS <sub>2</sub> /TiO <sub>2</sub>	Nanoparticle	~10	64.3%	485/0.5 A/g, 200th cycle	303/2 A/g	[141]
SnS <sub>2</sub> /graphene	Nanoparticle	3	74.4%	1480/0.2 A/g, 50th cycle	666/10 A/g	[159]
G-SnS <sub>2</sub>	Nanoplate	7	38%	650/50 mA/g, 30th cycle	230/6.4 A/g	[142]
SnS <sub>2</sub> /graphene	Nanoplate	2–5	69%	704/387 mA/g, 100th cycle	303/6.45 A/g	[155]
SnS <sub>2</sub> -G	Nanoplate	~3.6	73%	826/500 mA/g, 200th cycle	498/8 A/g	[151]
SnS <sub>2</sub> /G	Nanoplate	N/A	42.4%	920/100 mA/g, 50th cycle	600/1 A/g	[139]
SnS <sub>2</sub> /GAs	Nanoplate	200	37%	656/50 mA/g, 30th cycle	240/1 A/g	[150]
SnS <sub>2</sub> /graphene	Nanoplate	300	69%	1060/100 mA/g, 200th cycle	670/2 A/g	[148]
SnS <sub>2</sub> /G-CNT	Nanosheet	10–30	63%	1017/100 mA/g, 100th cycle	634.6/2 A/g	[170]
SnS <sub>2</sub> /GNS	Nanosheet	20–25	83.7%	1114/100 mA/g, 30th cycle	870/1 A/g	[145]
L-SnS <sub>2</sub> /G	Nanosheet	5	74.16%	773/200 mA/g, 180th cycle	567/2 A/g	[146]
SnS <sub>2</sub> -graphene	Nanosheet	N/A	~71%	570/0.2 C, 30th cycle	N/A	[153]
SnS <sub>2</sub> /RGO	Nanosheet	10	55.6%	514/1.2 A/g, 300th cycle	447/8 C	[157]
SnS <sub>2</sub> /RGO/SnS <sub>2</sub>	Nanosheet	4.43	81%	1357/100 mA/g, 200th cycle	844/10 A/g	[151]
SnS <sub>2</sub> @GT	Nanorod	10	57.3%	720/0.2 A/g, 350th cycle	247/5 A/g	[158]
SnS <sub>2</sub> @GF	Nanoflakes	N/A	69.6%	818.4/1 A/g, 500th cycle	160.9 /5 A/g	[144]
GNS@MoS <sub>2</sub> @SnS <sub>2</sub>	Nanoflakes	20	66%	743/80 mA/g, 100th cycle	710/320 mA/g	[152]
SnS <sub>2</sub> NF@RGO	Nanoflower	N/A	~78%	525/615.5 mA/g, 360th cycle	412.5/2462 mA/g	[49]

## 5. Summary and Outlook

SnS<sub>2</sub>/carbon composites have been considered as an appealing family of high-capacity anode materials for next-generation LIBs. This review provides a comprehensive overview of the most significant advances in their microstructure, Li storage instrument, combination, and electrochemical characteristics. Specific accentuation has been put on handling the rest of the issues of SnS<sub>2</sub>-based anode materials through a reasonable basic structure (i.e., building remarkable nanostructures, different morphology, and creating SnS<sub>2</sub>/carbon-based composites). Besides, different procedures can be taken for electrochemical execution upgrade, such as securing controlled pre-lithiation and polymer fastener enhancement.

The creators suggested that the micropores could adequately mitigate the volume changes of SnS<sub>2</sub> nanoparticles and forestall the breakdown of the permeable structure. The high explicit surface zone encourages the effective contact of dynamic materials with electrolytes. Among different carbon materials, compositing SnS<sub>2</sub> with graphene sheets is

one of the hotly debated ongoing exploration issues in recent years since the synergistic impact between SnS<sub>2</sub> and graphene can strikingly improve the anode's electrochemical performance. On the one hand, the graphene sheets could not just forestall the agglomeration of small SnS<sub>2</sub> particles, cradle the volume change during charge–release forms, and essentially upgrade the terminal's electronic conductivity. The diverse nanostructures of SnS<sub>2</sub>, including nanoparticles, nanorods/nanowires, nanosheets, nanoflowers, and 3D nanospheres, can also ease the volume change during the charge–release process.

In this paper, we focused on the morphological structure of the SnS<sub>2</sub> material. In the case of pure SnS<sub>2</sub>-based anodes, particle size has a significant impact on discharging capacity. SnS<sub>2</sub>, with smaller particle size, showed better capacity retention and discharging capacity, and also provided more a specific area for volume change expansion. Nanoflower based structures with more active sites for Li-ion insertion significantly improve capacity retention and discharging capability at high current rates. In case of hybrid materials, the specific area and morphology of the other component also play a vital role in capacity performance. As we discussed in the graphene section, sandwich-like nanosheet structures could reduce the Li-ion diffusion distance and have shown excellent CE and rate capability. However, the dispersion length of Li particles is an extremely important factor in improving the reversible limit and cycling dependability. Graphene-based materials are growing rapidly as an incredibly adaptable 2D material for electrochemical energy storage systems, which have aided batteries in achieving excellent high capacities and rate capability due to their optimized interlayer spacing and proprietary chemistry. These accomplishments are a result of graphene's inherent features, which include strong electrical conductivity, a defined structure, and the capacity to sustain adaptations, allowing for the electrodes to be tailored to a specific application.

There is still a long way to go before the use of SnS<sub>2</sub>/graphene composites. Although some of the procedures listed are fairly easy after obtaining graphene or GO, one of the major difficulties is the question of how to further simplify the process of manufacturing graphene. Furthermore, further work is required to alter the mechanical characteristics of the SEI layer, such as SnS<sub>2</sub>/graphene-active materials, binders, electrolytes, and electrolyte additives, in order to achieve improved cycle performance and CE (Figure 11). Meanwhile, high energy consumption in material and battery production, depletion of critical raw material resources, and low degradation rates are incompatible with the current sustainability of LIBs, and could result in a severe environmental impact and uncertain production conditions in the future, which also need to be taken under consideration for future work. However, it is certain that SnS<sub>2</sub>-based anode materials will make tremendous advances in the near future due to the ongoing and unwavering efforts throughout the world, which will play an increasingly essential and active role in next-generation high-energy-density LIBs.

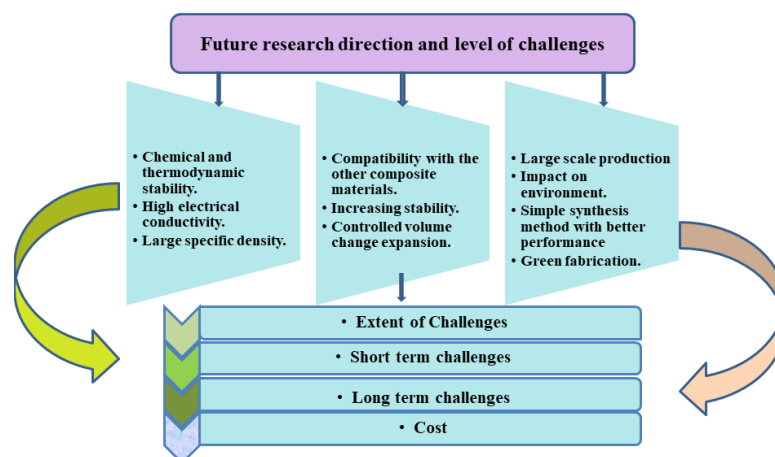


**Figure 11.** Future research direction and level of challenges.

**Author Contributions:** Conceptualization, S.T.M. and L.L.; materials organization, S.T.M., R.M. and S.M.; writing—original draft preparation, S.T.M., R.M. and S.M.; writing—review and editing, M.Y., L.L. and J.Z.; supervision, S.S. and L.L.; funding acquisition, L.L., R.Z. and Z.D. All authors have read and agreed to the published version of the manuscript.

**Funding:** This research was funded by the National Natural Science Foundation of China (No. 61802285), the Natural Science Foundation of Hubei Province (No. 2021CFB478), the Scientific Research Project of Hubei Provincial Department of Education (No. D20201704), the Key Research and Development Project of Hubei Province (No. 2020BAB076), the Hubei Province Technical Innovation Special Project (No. 2019AAA005), the Chinese Government CSC Scholarship Program (CSC Number: 2019SLJ019819 and 2019SLJ019821), and the Chutian Scholar Program of Hubei Province.

**Institutional Review Board Statement:** Not applicable.

**Informed Consent Statement:** Not applicable.

**Data Availability Statement:** Not applicable.

**Conflicts of Interest:** The authors declare no conflict of interest.

## References

1. Li, D.; Luo, L.; Zhu, J.; Qin, H.; Liu, P.; Sun, Z.; Lei, Y.; Jiang, M. A hybrid lithium sulfonated polyoxadiazole derived single-ion conducting gel polymer electrolyte enabled effective suppression of dendritic lithium growth. *Chin. Chem. Lett.* **2022**, *33*, 1025–1031. [[CrossRef](#)]
2. Li, D.; Wang, H.; Luo, L.; Zhu, J.; Li, J.; Liu, P.; Yu, Y.; Jiang, M. Electrospun Separator Based on Sulfonated Polyoxadiazole with Outstanding Thermal Stability and Electrochemical Properties for Lithium-Ion Batteries. *ACS Appl. Energy Mater.* **2021**, *4*, 879–887. [[CrossRef](#)]
3. Yu, Y.; Zhu, J.; Zeng, K.; Jiang, M. Mechanically robust and superior conductive n-type polymer binders for high-performance micro-silicon anodes in lithium-ion batteries. *J. Mater. Chem. A* **2021**, *9*, 3472–3481. [[CrossRef](#)]
4. Han, L.; Lehmann, M.L.; Zhu, J.; Liu, T.; Zhou, Z.; Tang, X.; Heish, C.-T.; Sokolov, A.P.; Cao, P.; Chen, X.C. Recent Developments and Challenges in Hybrid Solid Electrolytes for Lithium-Ion Batteries. *Front. Energy Res.* **2020**, *8*, 202. [[CrossRef](#)]
5. Gao, H.; Mao, J.; Li, D.; Yu, Y.; Yang, C.; Qi, S.; Liu, Q.; Zhu, J.; Jiang, M. Communication—Lithium sulfonated polyoxadiazole as a novel single-ion polymer electrolyte in lithium-ion batteries. *J. Electrochem. Soc.* **2020**, *167*, 070518. [[CrossRef](#)]
6. Yang, C.; Li, D.; Gao, H.; Liu, Q.; Zhu, J.; Wang, F.; Jiang, M. Constructing High-Energy-Density Aqueous Supercapacitors with Potassium Iodide-Doped Electrolytes by a Precharging Method. *ACS Appl. Energy Mater.* **2020**, *3*, 2674–2681. [[CrossRef](#)]
7. Huang, Z.X.; Wang, Y.; Liu, B.; Kong, D.; Zhang, J.; Chen, T.; Yang, H.Y. Unlocking the potential of SnS<sub>2</sub>: Transition metal catalyzed utilization of reversible conversion and alloying reactions. *Sci. Rep.* **2017**, *7*, 1–11. [[CrossRef](#)]
8. Whitesides, G.M.; Mathias, J.P.; Seto, C.T. Molecular self-assembly and nanochemistry: A chemical strategy for the synthesis of nanostructures. *Science* **1991**, *254*, 1312–1319. [[CrossRef](#)]
9. Liu, W.; Huang, X.; Wang, Z.; Li, H.; Chen, L. Studies of stannic oxide as an anode material for lithium-ion batteries. *J. Electrochem. Soc.* **1998**, *145*, 59. [[CrossRef](#)]
10. Palacin, M.R. Recent advances in rechargeable battery materials: A chemist’s perspective. *Chem. Soc. Rev.* **2009**, *38*, 2565–2575. [[CrossRef](#)]
11. Carny, O.; Shalev, D.E.; Gazit, E. Fabrication of coaxial metal nanocables using a self-assembled peptide nanotube scaffold. *Nano Lett.* **2006**, *6*, 1594–1597. [[CrossRef](#)] [[PubMed](#)]
12. Zhu, J.; Yildirim, E.; Aly, K.; Shen, J.; Chen, C.; Lu, Y.; Jiang, M.; Kim, D.; Tonelli, A.E.; Pasquinelli, M.A. Hierarchical multi-component nanofiber separators for lithium polysulfide capture in lithium–sulfur batteries: An experimental and molecular modeling study. *J. Mater. Chem. A* **2016**, *4*, 13572–13581. [[CrossRef](#)]
13. Yin, L.; Chai, S.; Ma, J.; Huang, J.; Kong, X.; Bai, P.; Liu, Y. Effects of binders on electrochemical properties of the SnS<sub>2</sub> nanostructured anode of the lithium-ion batteries. *J. Alloys Compd.* **2017**, *698*, 828–834. [[CrossRef](#)]
14. Choi, J.W.; Aurbach, D. Promise and reality of post-lithium-ion batteries with high energy densities. *Nat. Rev. Mater.* **2016**, *1*, 1–16. [[CrossRef](#)]
15. Goodenough, J.B.; Kim, Y. Challenges for rechargeable Li batteries. *Chem. Mater.* **2010**, *22*, 587–603. [[CrossRef](#)]
16. Li, X.; Lu, Y.; Hou, Z.; Zhang, W.; Zhu, Y.; Qian, Y.; Liang, J.; Qian, Y. SnS<sub>2</sub>-compared to SnO<sub>2</sub>-stabilized S/C composites toward high-performance lithium sulfur batteries. *ACS Appl. Mater. Interfaces* **2016**, *8*, 19550–19557. [[CrossRef](#)]
17. Son, I.H.; Park, J.H.; Park, S.; Park, K.; Han, S.; Shin, J.; Doo, S.-G.; Hwang, Y.; Chang, H.; Choi, J.W. Graphene balls for lithium rechargeable batteries with fast charging and high volumetric energy densities. *Nat. Commun.* **2017**, *8*, 1–11. [[CrossRef](#)]
18. O’Heir, J. Building better batteries. *Mech. Eng.* **2017**, *139*, 10.
19. Choi, S.; Kwon, T.-W.; Coskun, A.; Choi, J.W. Highly elastic binders integrating polyrotaxanes for silicon microparticle anodes in lithium ion batteries. *Science* **2017**, *357*, 279–283. [[CrossRef](#)]

20. Yazami, R.; Touzain, P. A reversible graphite-lithium negative electrode for electrochemical generators. *J. Power Sources* **1983**, *9*, 365–371. [[CrossRef](#)]
21. Zaghbi, K.; Simoneau, M.; Armand, M.; Gauthier, M. Electrochemical study of  $\text{Li}_4\text{Ti}_5\text{O}_{12}$  as negative electrode for Li-ion polymer rechargeable batteries. *J. Power Sources* **1999**, *81*, 300–305. [[CrossRef](#)]
22. Choi, S.; Cho, Y.G.; Kim, J.; Choi, N.S.; Song, H.K.; Wang, G.; Park, S. Mesoporous Germanium Anode Materials for Lithium-Ion Battery with Exceptional Cycling Stability in Wide Temperature Range. *Small* **2017**, *13*, 1603045. [[CrossRef](#)] [[PubMed](#)]
23. Meister, P.; Jia, H.; Li, J.; Kloepsch, R.; Winter, M.; Placke, T. Best practice: Performance and cost evaluation of lithium ion battery active materials with special emphasis on energy efficiency. *Chem. Mater.* **2016**, *28*, 7203–7217. [[CrossRef](#)]
24. Guo, J.; Dong, D.; Wang, J.; Liu, D.; Li, D.; Yu, X.; Zheng, Y.; Wen, Z.; Lei, W.; Deng, Y.; et al. Silicon-Based Lithium Ion Battery Systems: State-of-the-Art from Half and Full Cell Viewpoint. *Adv. Funct. Mater.* **2021**, *31*, 2102546. [[CrossRef](#)]
25. Zhang, C.; Mahmood, N.; Yin, H.; Liu, F.; Hou, Y. Synthesis of phosphorus-doped graphene and its multifunctional applications for oxygen reduction reaction and lithium ion batteries. *Adv. Mater.* **2013**, *25*, 4932–4937. [[CrossRef](#)] [[PubMed](#)]
26. Wang, L.; He, X.; Li, J.; Sun, W.; Gao, J.; Guo, J.; Jiang, C. Nano-structured phosphorus composite as high-capacity anode materials for lithium batteries. *Angew. Chem.* **2012**, *124*, 9168–9171. [[CrossRef](#)]
27. Zeng, Z.; Sun, T.; Zhu, J.; Huang, X.; Yin, Z.; Lu, G.; Fan, Z.; Yan, Q.; Hng, H.H.; Zhang, H. An effective method for the fabrication of few-layer-thick inorganic nanosheets. *Angew. Chem. Int. Ed.* **2012**, *51*, 9052–9056. [[CrossRef](#)] [[PubMed](#)]
28. Luo, W.; Zhang, P.; Wang, X.; Li, Q.; Dong, Y.; Hua, J.; Zhou, L.; Mai, L. Antimony nanoparticles anchored in three-dimensional carbon network as promising sodium-ion battery anode. *J. Power Sources* **2016**, *304*, 340–345. [[CrossRef](#)]
29. Prikhodchenko, P.V.; Gun, J.; Sladkevich, S.; Mikhaylov, A.A.; Lev, O.; Tay, Y.Y.; Batabyal, S.K.; Yu, D.Y. Conversion of hydroperoxoantimonate coated graphenes to  $\text{Sb}_2\text{S}_3$ @ graphene for a superior lithium battery anode. *Chem. Mater.* **2012**, *24*, 4750–4757. [[CrossRef](#)]
30. Li, J.; Tang, S.; Lu, L.; Zeng, H.C. Preparation of nanocomposites of metals, metal oxides, and carbon nanotubes via self-assembly. *J. Am. Chem. Soc.* **2007**, *129*, 9401–9409. [[CrossRef](#)]
31. Hayner, C.M.; Zhao, X.; Kung, H.H. Materials for rechargeable lithium-ion batteries. *Annu. Rev. Chem. Biomol. Eng.* **2012**, *3*, 445–471. [[CrossRef](#)] [[PubMed](#)]
32. Tirado, J.L. Inorganic materials for the negative electrode of lithium-ion batteries: State-of-the-art and future prospects. *Mater. Sci. Eng. R Rep.* **2003**, *40*, 103–136. [[CrossRef](#)]
33. Lee, W.-G.; Jang, H.S.; Raj, C.J.; Rajesh, M.; Kim, B.C.; Cho, W.-J.; Yu, K.H. Effect of proton irradiation on the structural and electrochemical properties of  $\text{MnO}_2$  nanosheets. *J. Electroanal. Chem.* **2018**, *811*, 16–25. [[CrossRef](#)]
34. Gund, G.S.; Dubal, D.P.; Patil, B.H.; Shinde, S.S.; Lokhande, C.D. Enhanced activity of chemically synthesized hybrid graphene oxide/ $\text{Mn}_3\text{O}_4$  composite for high performance supercapacitors. *Electrochim. Acta* **2013**, *92*, 205–215. [[CrossRef](#)]
35. Li, W.; Shao, J.; Liu, Q.; Liu, X.; Zhou, X.; Hu, J. Facile synthesis of porous  $\text{Mn}_2\text{O}_3$  nanocubics for high-rate supercapacitors. *Electrochim. Acta* **2015**, *157*, 108–114. [[CrossRef](#)]
36. Deng, Y.; Wan, L.; Xie, Y.; Qin, X.; Chen, G. Recent advances in Mn-based oxides as anode materials for lithium ion batteries. *RSC Adv.* **2014**, *4*, 23914–23935. [[CrossRef](#)]
37. Yang, L.; Hu, J.; Dong, A.; Yang, D. Novel  $\text{Fe}_3\text{O}_4$ -CNTs nanocomposite for Li-ion batteries with enhanced electrochemical performance. *Electrochim. Acta* **2014**, *144*, 235–242. [[CrossRef](#)]
38. Balogun, M.-S.; Wu, Z.; Luo, Y.; Qiu, W.; Fan, X.; Long, B.; Huang, M.; Liu, P.; Tong, Y. High power density nitrated hematite ( $\alpha$ - $\text{Fe}_2\text{O}_3$ ) nanorods as anode for high-performance flexible lithium ion batteries. *J. Power Sources* **2016**, *308*, 7–17. [[CrossRef](#)]
39. Xiong, S.; Chen, J.S.; Lou, X.W.; Zeng, H.C. Mesoporous  $\text{Co}_3\text{O}_4$  and  $\text{CoO@C}$  topotactically transformed from chrysanthemum-like  $\text{Co}(\text{CO}_3)_{0.5}(\text{OH})\cdot 0.11 \text{H}_2\text{O}$  and their lithium-storage properties. *Adv. Funct. Mater.* **2012**, *22*, 861–871. [[CrossRef](#)]
40. Khalil, A.; Lalia, B.S.; Hashaikeh, R. Nickel oxide nanocrystals as a lithium-ion battery anode: Structure-performance relationship. *J. Mater. Sci.* **2016**, *51*, 6624–6638. [[CrossRef](#)]
41. Zhao, Q.; Ma, L.; Zhang, Q.; Wang, C.; Xu, X.  $\text{SnO}_2$ -based nanomaterials: Synthesis and application in lithium-ion batteries and supercapacitors. *J. Nanomater.* **2015**, *2015*, 1–15. [[CrossRef](#)]
42. Li, R.; Miao, C.; Yu, L.; Zhang, M.; Xiao, W. Novel self-assembled  $\text{SnO}_2$ @  $\text{SnS}_2$  hybrid microspheres as potential anode materials for lithium-ion batteries. *Mater. Lett.* **2020**, *272*, 127851. [[CrossRef](#)]
43. Khan, Z.; Parveen, N.; Ansari, S.A.; Senthilkumar, S.T.; Park, S.; Kim, Y.; Cho, M.H.; Ko, H. Three-dimensional  $\text{SnS}_2$  nanopetals for hybrid sodium-air batteries. *Electrochim. Acta* **2017**, *257*, 328–334. [[CrossRef](#)]
44. Liu, J.; Chen, X.; Zeng, L.; He, X.; Liu, J.; Huang, B.; Xiao, L.; Qian, Q.; Wei, M.; Chen, Q.  $\text{SnS}_2$  nanosheets anchored on porous carbon fibers for high performance of sodium-ion batteries. *J. Electroanal. Chem.* **2020**, *862*, 114021. [[CrossRef](#)]
45. Lefebvre-Devos, I.; Olivier-Fourcade, J.; Jumas, J.; Lavela, P. Lithium insertion mechanism in  $\text{SnS}_2$ . *Phys. Rev. B* **2000**, *61*, 3110. [[CrossRef](#)]
46. Jiang, T.; Ozin, G.A. New directions in tin sulfide materials chemistry. *J. Mater. Chem.* **1998**, *8*, 1099–1108. [[CrossRef](#)]
47. Morales, J.; Vicente, C.P.; Santos, J.; Tirado, J. Electrochemical characteristics of crystalline and amorphous  $\text{SnS}_2$  in lithium cells. *J. Electrochem. Soc.* **1996**, *143*, 2847. [[CrossRef](#)]
48. Cheng, Y.; Xie, H.; Zhou, L.; Shi, B.; Guo, L.; Huang, J. In-situ liquid-phase transformation of  $\text{SnS}_2$ /CNTs composite from  $\text{SnO}_2$ /CNTs for high performance lithium-ion battery anode. *Appl. Surf. Sci.* **2021**, *566*, 150645. [[CrossRef](#)]

49. Liu, J.; Qi, Y.; Fu, B.; Dai, J.; Wang, Q.; Zhu, X.; Shi, X. Li<sup>+</sup> diffusion kinetics of SnS<sub>2</sub> nanoflowers enhanced by reduced graphene oxides with excellent electrochemical performance as anode material for lithium-ion batteries. *J. Alloys Compd.* **2019**, *794*, 285–293. [[CrossRef](#)]
50. Kim, T.-J.; Kim, C.; Son, D.; Choi, M.; Park, B. Novel SnS<sub>2</sub>-nanosheet anodes for lithium-ion batteries. *J. Power Sources* **2007**, *167*, 529–535. [[CrossRef](#)]
51. Wang, Y.; Zhou, J.; Wu, J.; Chen, F.; Li, P.; Han, N.; Huang, W.; Liu, Y.; Ye, H.; Zhao, F.; et al. Engineering SnS<sub>2</sub> nanosheet assemblies for enhanced electrochemical lithium and sodium ion storage. *J. Mater. Chem. A* **2017**, *5*, 25618–25624. [[CrossRef](#)]
52. Cui, Z.; He, S.; Liu, Q.; Guan, G.; Zhang, W.; Xu, C.; Zhu, J.; Feng, P.; Hu, J.; Zou, R.; et al. Graphene-Like Carbon Film Wrapped Tin (II) Sulfide Nanosheet Arrays on Porous Carbon Fibers with Enhanced Electrochemical Kinetics as High-Performance Li and Na Ion Battery Anodes. *Adv. Sci.* **2020**, *7*, 1903045. [[CrossRef](#)] [[PubMed](#)]
53. Ji, L.; Xin, H.L.; Kuykendall, T.R.; Wu, S.-L.; Zheng, H.; Rao, M.; Cairns, E.J.; Battaglia, V.; Zhang, Y. SnS<sub>2</sub> nanoparticle loaded graphene nanocomposites for superior energy storage. *Phys. Chem. Chem. Phys.* **2012**, *14*, 6981–6986. [[CrossRef](#)] [[PubMed](#)]
54. Shen, C.; Ma, L.; Zheng, M.; Zhao, B.; Qiu, D.; Pan, L.; Cao, J.; Shi, Y. Synthesis and electrochemical properties of graphene-SnS<sub>2</sub> nanocomposites for lithium-ion batteries. *J. Solid State Electrochem.* **2012**, *16*, 1999–2004. [[CrossRef](#)]
55. Liu, Y.; Yu, X.-Y.; Fang, Y.; Zhu, X.; Bao, J.; Zhou, X.; Lou, X.W.D. Confining SnS<sub>2</sub> ultrathin nanosheets in hollow carbon nanostructures for efficient capacitive sodium storage. *Joule* **2018**, *2*, 725–735. [[CrossRef](#)]
56. Zhang, Z.; Zhao, H.; Du, Z.; Chang, X.; Zhao, L.; Du, X.; Li, Z.; Teng, Y.; Fang, J.; Swierczek, K. (101) Plane-oriented SnS<sub>2</sub> nanoplates with carbon coating: A high-rate and cycle-stable anode material for lithium ion batteries. *ACS Appl. Mater. Interfaces* **2017**, *9*, 35880–35887. [[CrossRef](#)]
57. Cui, J.; Yao, S.; Lu, Z.; Huang, J.; Chong, W.G.; Ciucci, F.; Kim, J. Revealing Pseudocapacitive Mechanisms of Meta Dichalcogenide SnS<sub>2</sub>/Graphene-CNT Aerogels for High-Energy Na Hybrid Capacitors. *Adv. Energy Mater.* **2018**, *8*, 1702488. [[CrossRef](#)]
58. Hwang, S.; Yao, Z.; Zhang, L.; Fu, M.; He, K.; Mai, L.; Wolverton, C.; Su, D. Multistep lithiation of tin sulfide: An investigation using in situ electron microscopy. *ACS Nano* **2018**, *12*, 3638–3645. [[CrossRef](#)]
59. Liang, C.; Gao, M.; Pan, H.; Liu, Y.; Yan, M. Lithium alloys and metal oxides as high-capacity anode materials for lithium-ion batteries. *J. Alloys Compd.* **2013**, *575*, 246–256. [[CrossRef](#)]
60. Gao, C.; Li, L.; Raji, A.R.; Kovalchuk, A.; Peng, Z.; Fei, H.; He, Y.; Kim, N.D.; Zhong, Q.; Xie, E.; et al. Tin Disulfide Nanoplates on Graphene Nanoribbons for Full Lithium Ion Batteries. *ACS Appl. Mater. Interfaces* **2015**, *7*, 26549–26556. [[CrossRef](#)]
61. Bala, M.; Masarrat, A.; Bhogra, A.; Meena, R.; Lu, Y.-R.; Huang, Y.-C.; Chen, C.-L.; Dong, C.-L.; Ojha, S.; Avasthi, D. Structure and Transport Properties of Nickel-Implanted CoSb<sub>3</sub> Skutterudite Thin Films Synthesized via Pulsed Laser Deposition. *ACS Appl. Energy Mater.* **2018**, *1*, 5879–5886. [[CrossRef](#)]
62. Liu, Z.; Deng, H.; Mukherjee, P.P. Evaluating pristine and modified SnS<sub>2</sub> as a lithium-ion battery anode: A first-principles study. *ACS Appl. Mater. Interfaces* **2015**, *7*, 4000–4009. [[CrossRef](#)] [[PubMed](#)]
63. Gonzalez, J.M.; Oleynik, I.I. Layer-dependent properties of SnS<sub>2</sub> and SnSe<sub>2</sub> two-dimensional materials. *Phys. Rev. B* **2016**, *94*, 125443. [[CrossRef](#)]
64. Deng, Y.; Fang, C.; Chen, G. The developments of SnO<sub>2</sub>/graphene nanocomposites as anode materials for high performance lithium ion batteries: A review. *J. Power Sources* **2016**, *304*, 81–101. [[CrossRef](#)]
65. Liu, Y.; Wang, Y.M.; Jakobson, B.I.; Wood, B.C. Assessing carbon-based anodes for lithium-ion batteries: A universal description of charge-transfer binding. *Phys. Rev. Lett.* **2014**, *113*, 028304. [[CrossRef](#)]
66. Liu, S.; Yin, X.; Chen, L.; Li, Q.; Wang, T. Synthesis of self-assembled 3D flowerlike SnS<sub>2</sub> nanostructures with enhanced lithium ion storage property. *Solid State Sci.* **2010**, *12*, 712–718. [[CrossRef](#)]
67. Mukaibo, H.; Yoshizawa, A.; Momma, T.; Osaka, T. Particle size and performance of SnS<sub>2</sub> anodes for rechargeable lithium batteries. *J. Power Sources* **2003**, *119*, 60–63. [[CrossRef](#)]
68. Zuo, Y.; Xu, X.; Zhang, C.; Li, J.; Du, R.; Wang, X.; Han, X.; Arbiol, J.; Llorca, J.; Liu, J. SnS<sub>2</sub>/g-C<sub>3</sub>N<sub>4</sub>/graphite nanocomposites as durable lithium-ion battery anode with high pseudocapacitance contribution. *Electrochim. Acta* **2020**, *349*, 136369. [[CrossRef](#)]
69. Liu, H.; Wei, C.; Ai, Z.; Li, M.; Xu, M.; Ma, C.; Shi, J. The positive effect of 3D interpenetrating network porous structure by carbon membranes on alleviating the volume expansion of SnS<sub>2</sub> nanosheets for enhancing lithium and sodium storage. *Colloids Surf. A Physicochem. Eng. Asp.* **2021**, *610*, 125937. [[CrossRef](#)]
70. Wang, C.; Zhang, Y.; Li, Y.; Zhang, Y.; Dong, Y.; Li, D.; Zhang, J. Construction of uniform SnS<sub>2</sub>/ZnS heterostructure nanosheets embedded in graphene for advanced lithium-ion batteries. *J. Alloys Compd.* **2020**, *820*, 153147. [[CrossRef](#)]
71. Hao, Y.; Wang, S.; Shao, Y.; Wu, Y.; Miao, S. High-Energy Density Li-Ion Capacitor with Layered SnS<sub>2</sub>/Reduced Graphene Oxide Anode and BCN Nanosheet Cathode. *Adv. Energy Mater.* **2020**, *10*, 1902836. [[CrossRef](#)]
72. Sun, D.; Wang, M.; Li, Z.; Fan, G.; Fan, L.-Z.; Zhou, A. Two-dimensional Ti<sub>3</sub>C<sub>2</sub> as anode material for Li-ion batteries. *Electrochem. Commun.* **2014**, *47*, 80–83. [[CrossRef](#)]
73. Wang, Q.; Huang, Y.; Miao, J.; Zhao, Y.; Wang, Y. Synthesis and electrochemical characterizations of Ce doped SnS<sub>2</sub> anode materials for rechargeable lithium ion batteries. *Electrochim. Acta* **2013**, *93*, 120–130. [[CrossRef](#)]
74. Chen, Q.; Lu, F.; Xia, Y.; Wang, H.; Kuang, X. Interlayer expansion of few-layered Mo-doped SnS<sub>2</sub> nanosheets grown on carbon cloth with excellent lithium storage performance for lithium ion batteries. *J. Mater. Chem. A* **2017**, *5*, 4075–4083. [[CrossRef](#)]

75. McNair, O.D.; Brent, D.P.; Sparks, B.J.; Patton, D.L.; Savin, D.A. Sequential thiol click reactions: Formation of ternary thiourethane/thiol-ene networks with enhanced thermal and mechanical properties. *ACS Appl. Mater. Interfaces* **2014**, *6*, 6088–6097. [[CrossRef](#)]
76. Wu, Z.-S.; Zhou, G.; Yin, L.-C.; Ren, W.; Li, F.; Cheng, H.-M. Graphene/metal oxide composite electrode materials for energy storage. *Nano Energy* **2012**, *1*, 107–131. [[CrossRef](#)]
77. Zhou, H.; Zhang, L.; Zhang, D.; Chen, S.; Coxon, P.R.; He, X.; Coto, M.; Kim, H.-K.; Xi, K.; Ding, S. A universal synthetic route to carbon nanotube/transition metal oxide nano-composites for lithium ion batteries and electrochemical capacitors. *Sci. Rep.* **2016**, *6*, 1–11. [[CrossRef](#)]
78. Fang, H.; Zhao, L.; Yue, W.; Wang, Y.; Jiang, Y.; Zhang, Y. Facile and large-scale preparation of sandwich-structured graphene-metal oxide composites as anode materials for Li-ion batteries. *Electrochim. Acta* **2015**, *186*, 397–403. [[CrossRef](#)]
79. Greenaway, D.L.; Nitsche, R. Preparation and optical properties of group IV–VI2 chalcogenides having the CdI<sub>2</sub> structure. *J. Phys. Chem. Solids* **1965**, *26*, 1445–1458. [[CrossRef](#)]
80. Deshpande, N.; Sagade, A.; Gudage, Y.; Lokhande, C.; Sharma, R. Growth and characterization of tin disulfide (SnS<sub>2</sub>) thin film deposited by successive ionic layer adsorption and reaction (SILAR) technique. *J. Alloys Compd.* **2007**, *436*, 421–426. [[CrossRef](#)]
81. Huang, Y.; Ling, C.; Chen, X.; Zhou, D.; Wang, S. SnS<sub>2</sub> nanotubes: A promising candidate for the anode material for lithium ion batteries. *RSC Adv.* **2015**, *5*, 32505–32510. [[CrossRef](#)]
82. Ray, S.C.; Karanjai, M.K.; DasGupta, D. Structure and photoconductive properties of dip-deposited SnS and SnS<sub>2</sub> thin films and their conversion to tin dioxide by annealing in air. *Thin Solid Film* **1999**, *350*, 72–78. [[CrossRef](#)]
83. Hassan, A.S.; Moyer, K.; Ramachandran, B.R.; Wick, C.D. Comparison of storage mechanisms in RuO<sub>2</sub>, SnO<sub>2</sub>, and SnS<sub>2</sub> for lithium-ion battery anode materials. *J. Phys. Chem. C* **2016**, *120*, 2036–2046. [[CrossRef](#)]
84. Francis, L. *Crystallography and Crystal Chemistry of Materials with Layered Structures*; D. Reidel Publishing Company: Dordrecht, The Netherlands, 1976.
85. Brousse, T.; Lee, S.; Pasquereau, L.; Defives, D.; Schleich, D. Composite negative electrodes for lithium ion cells. *Solid State Ion.* **1998**, *113*, 51–56. [[CrossRef](#)]
86. Marestoni, L.D.; Barud, H.D.S.; Gomes, R.J.; Catarino, R.P.F.; Hata, N.N.Y.; Ressutte, J.B.; Spinosa, W.A. Commercial and potential applications of bacterial cellulose in Brazil: Ten years review. *Polímeros* **2021**, *30*, 1–19. [[CrossRef](#)]
87. Wu, Y.; Zhao, Y.; Meng, W.; Xie, Y.; Zhang, J.; He, C.; Zhao, D. Nanoplates-assembled SnS<sub>2</sub> nanoflowers with carbon coating anchored on reduced graphene oxide for high performance Li-ion batteries. *Appl. Surf. Sci.* **2021**, *539*, 148283. [[CrossRef](#)]
88. Soto, F.A.; Ma, Y.; Martinez De La Hoz, J.M.; Seminario, J.M.; Balbuena, P.B. Formation and growth mechanisms of solid-electrolyte interphase layers in rechargeable batteries. *Chem. Mater.* **2015**, *27*, 7990–8000. [[CrossRef](#)]
89. Xu, K. Nonaqueous liquid electrolytes for lithium-based rechargeable batteries. *Chem. Rev.* **2004**, *104*, 4303–4418. [[CrossRef](#)]
90. He, Y.-B.; Liu, M.; Huang, Z.-D.; Zhang, B.; Yu, Y.; Li, B.; Kang, F.; Kim, J.-K. Effect of solid electrolyte interface (SEI) film on cyclic performance of Li<sub>4</sub>Ti<sub>5</sub>O<sub>12</sub> anodes for Li ion batteries. *J. Power Sources* **2013**, *239*, 269–276. [[CrossRef](#)]
91. Aurbach, D. Review of selected electrode–solution interactions which determine the performance of Li and Li ion batteries. *J. Power Sources* **2000**, *89*, 206–218. [[CrossRef](#)]
92. Momma, T.; Shiraiishi, N.; Yoshizawa, A.; Osaka, T.; Gedanken, A.; Zhu, J.; Sominski, L. SnS<sub>2</sub> anode for rechargeable lithium battery. *J. Power Sources* **2001**, *97*, 198–200. [[CrossRef](#)]
93. Thangavel, R.; Samuthira Pandian, A.; Ramasamy, H.V.; Lee, Y.-S. Rapidly synthesized, few-layered pseudocapacitive SnS<sub>2</sub> anode for high-power sodium ion batteries. *ACS Appl. Mater. Interfaces* **2017**, *9*, 40187–40196. [[CrossRef](#)] [[PubMed](#)]
94. Seo, J.w.; Jang, J.t.; Park, S.w.; Kim, C.; Park, B.; Cheon, J. Two-dimensional SnS<sub>2</sub> nanoplates with extraordinary high discharge capacity for lithium ion batteries. *Adv. Mater.* **2008**, *20*, 4269–4273. [[CrossRef](#)]
95. Zai, J.; Wang, K.; Su, Y.; Qian, X.; Chen, J. High stability and superior rate capability of three-dimensional hierarchical SnS<sub>2</sub> microspheres as anode material in lithium ion batteries. *J. Power Sources* **2011**, *196*, 3650–3654. [[CrossRef](#)]
96. Wang, L.; Zhuo, L.; Yu, Y.; Zhao, F. High-rate performance of SnS<sub>2</sub> nanoplates without carbon-coating as anode material for lithium ion batteries. *Electrochim. Acta* **2013**, *112*, 439–447. [[CrossRef](#)]
97. Du, Y.; Yin, Z.; Rui, X.; Zeng, Z.; Wu, X.-J.; Liu, J.; Zhu, Y.; Zhu, J.; Huang, X.; Yan, Q. A facile, relative green, and inexpensive synthetic approach toward large-scale production of SnS<sub>2</sub> nanoplates for high-performance lithium-ion batteries. *Nanoscale* **2013**, *5*, 1456–1459. [[CrossRef](#)] [[PubMed](#)]
98. Liu, S.; Yin, X.; Hao, Q.; Zhang, M.; Li, L.; Chen, L.; Li, Q.; Wang, Y.; Wang, T. Chemical bath deposition of SnS<sub>2</sub> nanowall arrays with improved electrochemical performance for lithium ion battery. *Mater. Lett.* **2010**, *64*, 2350–2353. [[CrossRef](#)]
99. Zhong, H.; Yang, G.; Song, H.; Liao, Q.; Cui, H.; Shen, P.; Wang, C.-X. Vertically aligned graphene-like SnS<sub>2</sub> ultrathin nanosheet arrays: Excellent energy storage, catalysis, photoconduction, and field-emitting performances. *J. Phys. Chem. C* **2012**, *116*, 9319–9326. [[CrossRef](#)]
100. Zou, Y.; Wang, Y. Microwave solvothermal synthesis of flower-like SnS<sub>2</sub> and SnO<sub>2</sub> nanostructures as high-rate anodes for lithium ion batteries. *Chem. Eng. J.* **2013**, *229*, 183–189. [[CrossRef](#)]
101. Guan, D.; Li, J.; Gao, X.; Xie, Y.; Yuan, C. Growth characteristics and influencing factors of 3D hierarchical flower-like SnS<sub>2</sub> nanostructures and their superior lithium-ion intercalation performance. *J. Alloys Compd.* **2016**, *658*, 190–197. [[CrossRef](#)]
102. Wu, Q.; Jiao, L.; Du, J.; Yang, J.; Guo, L.; Liu, Y.; Wang, Y.; Yuan, H. One-pot synthesis of three-dimensional SnS<sub>2</sub> hierarchitectures as anode material for lithium-ion batteries. *J. Power Sources* **2013**, *239*, 89–93. [[CrossRef](#)]

103. Chen, X.; Jiang, H.; Pei, Y.; Chen, Y.; Zeng, Y.; Guo, H. Binder-free ultrathin SnS<sub>2</sub> with superior reversibility of conversion reaction for high-rate lithium ion batteries. *J. Alloys Compd.* **2021**, *873*, 159623. [[CrossRef](#)]
104. Qian, X.; Zhang, X.; Wang, C.; Wang, W.; Xie, Y.; Qian, Y. Solvent-thermal preparation of nanocrystalline tin chalcogenide. *J. Phys. Chem. Solids* **1999**, *60*, 415–417. [[CrossRef](#)]
105. Su, H.; Xie, Y.; Xiong, Y.; Gao, P.; Qian, Y. Preparation and morphology control of rod-like nanocrystalline tin sulfides via a simple ethanol thermal route. *J. Solid State Chem.* **2001**, *161*, 190–196. [[CrossRef](#)]
106. Ji, Y.; Zhang, H.; Ma, X.; Xu, J.; Yang, D. Single-crystalline SnS<sub>2</sub> nano-belts fabricated by a novel hydrothermal method. *J. Phys. Condens. Matter* **2003**, *15*, L661. [[CrossRef](#)]
107. Chen, D.; Shen, G.-Z.; Tang, K.-B.; Liu, Y.-K.; Qian, Y.-T. Aligned SnS<sub>2</sub> nanotubes fabricated via a template-assisted solvent-relief process. *Appl. Phys. A* **2003**, *77*, 747–749. [[CrossRef](#)]
108. Li, Q.; Ding, Y.; Wu, H.; Liu, X.; Qian, Y. Fabrication of layered nanocrystallites SnS and β-SnS<sub>2</sub> via a mild solution route. *Mater. Res. Bull.* **2002**, *37*, 925–932. [[CrossRef](#)]
109. Shen, G.; Chen, D.; Tang, K.; Huang, L.; Qian, Y.; Zhou, G. Novel polyol route to nanoscale tin sulfides flaky crystallines. *Inorg. Chem. Commun.* **2003**, *6*, 178–180. [[CrossRef](#)]
110. Chen, D.; Shen, G.; Tang, K.; Lei, S.; Zheng, H.; Qian, Y. Microwave-assisted polyol synthesis of nanoscale SnS<sub>x</sub> (x = 1, 2) flakes. *J. Cryst. Growth* **2004**, *260*, 469–474. [[CrossRef](#)]
111. Chen, X.; Lin, J.; Chen, Y.; Zhang, J.; Jiang, H.; Qiu, F.; Chu, R.; Guo, H. Binder-free and self-supported reduced graphene oxide coated Cu<sub>2</sub>SnS<sub>3</sub>/Carbon nanofibers for superior lithium storage. *J. Alloys Compd.* **2020**, *842*, 155619. [[CrossRef](#)]
112. Nath, M.; Rao, C.N.R. New metal disulfide nanotubes. *J. Am. Chem. Soc.* **2001**, *123*, 4841–4842. [[CrossRef](#)] [[PubMed](#)]
113. Mdleleni, M.M.; Hyeon, T.; Suslick, K.S. Sonochemical synthesis of nanostructured molybdenum sulfide. *J. Am. Chem. Soc.* **1998**, *120*, 6189–6190. [[CrossRef](#)]
114. Zhou, X.; Jin, B.; Yang, M.; Schmuki, P. MoS<sub>2</sub> Decorated on Different Metal Oxide Nanotubular Structures with a High Density of Reactive Sites for HER Reactions. In Proceedings of the ECS Meeting Abstracts, Seattle, WA, USA, 13–17 May 2018; p. 1709.
115. Guo, Y.G.; Hu, J.S.; Wan, L.J. Nanostructured materials for electrochemical energy conversion and storage devices. *Adv. Mater.* **2008**, *20*, 2878–2887. [[CrossRef](#)]
116. Ma, J.; Lei, D.; Duan, X.; Li, Q.; Wang, T.; Cao, A.; Mao, Y.; Zheng, W. Designable fabrication of flower-like SnS<sub>2</sub> aggregates with excellent performance in lithium-ion batteries. *RSC Adv.* **2012**, *2*, 3615–3617. [[CrossRef](#)]
117. Hao, J.; Wang, Y.; Chi, C.; Wang, J.; Guo, Q.; Yang, Y.; Li, Y.; Liu, X.; Zhao, J. Enhanced storage capability by biomass-derived porous carbon for lithium-ion and sodium-ion battery anodes. *Sustain. Energy Fuels* **2018**, *2*, 2358–2365. [[CrossRef](#)]
118. Hong, K.-l.; Qie, L.; Zeng, R.; Yi, Z.-q.; Zhang, W.; Wang, D.; Yin, W.; Wu, C.; Fan, Q.-j.; Zhang, W.-x. Biomass derived hard carbon used as a high performance anode material for sodium ion batteries. *J. Mater. Chem. A* **2014**, *2*, 12733–12738. [[CrossRef](#)]
119. Wang, P.; Zhu, X.; Wang, Q.; Xu, X.; Zhou, X.; Bao, J. Kelp-derived hard carbons as advanced anode materials for sodium-ion batteries. *J. Mater. Chem. A* **2017**, *5*, 5761–5769. [[CrossRef](#)]
120. Lu, P.; Sun, Y.; Xiang, H.; Liang, X.; Yu, Y. 3D amorphous carbon with controlled porous and disordered structures as a high-rate anode material for sodium-ion batteries. *Adv. Energy Mater.* **2018**, *8*, 1702434. [[CrossRef](#)]
121. Kim, H.S.; Chung, Y.H.; Kang, S.H.; Sung, Y.-E. Electrochemical behavior of carbon-coated SnS<sub>2</sub> for use as the anode in lithium-ion batteries. *Electrochim. Acta* **2009**, *54*, 3606–3610. [[CrossRef](#)]
122. Zhao, H.; Zeng, H.; Wu, Y.; Qi, W.; Zhang, S.; Li, B.; Huang, Y. Facile ball-milled synthesis of SnS<sub>2</sub>-carbon nanocomposites with superior lithium storage. *Prog. Nat. Sci. Mater. Int.* **2018**, *28*, 676–682. [[CrossRef](#)]
123. Li, J.; Wu, P.; Lou, F.; Zhang, P.; Tang, Y.; Zhou, Y.; Lu, T. Mesoporous carbon anchored with SnS<sub>2</sub> nanosheets as an advanced anode for lithium-ion batteries. *Electrochim. Acta* **2013**, *111*, 862–868. [[CrossRef](#)]
124. He, Y.; Xu, Z. The status and development of treatment techniques of typical waste electrical and electronic equipment in China: A review. *Waste Manag. Res.* **2014**, *32*, 254–269. [[CrossRef](#)] [[PubMed](#)]
125. Li, R.; Miao, C.; Zhang, M.; Xiao, W. Novel hierarchical structural SnS<sub>2</sub> composite supported by biochar carbonized from chewed sugarcane as enhanced anodes for lithium ion batteries. *Ionics* **2020**, *26*, 1239–1247. [[CrossRef](#)]
126. Zhai, C.; Du, N.; Zhang, H.; Yu, J.; Yang, D. Multiwalled carbon nanotubes anchored with SnS<sub>2</sub> nanosheets as high-performance anode materials of lithium-ion batteries. *ACS Appl. Mater. Interfaces* **2011**, *3*, 4067–4074. [[CrossRef](#)]
127. Chen, X.; Huang, Y.; Zhang, K.; Feng, X.; Wang, M. Synthesis and high-performance of carbonaceous polypyrrole nanotubes coated with SnS<sub>2</sub> nanosheets anode materials for lithium ion batteries. *Chem. Eng. J.* **2017**, *330*, 470–479. [[CrossRef](#)]
128. Wang, Y.; Zeng, H.C.; Lee, J.Y. Highly reversible lithium storage in porous SnO<sub>2</sub> nanotubes with coaxially grown carbon nanotube overlayers. *Adv. Mater.* **2006**, *18*, 645–649. [[CrossRef](#)]
129. Shin, H.C.; Liu, M. Three-dimensional porous copper-tin alloy electrodes for rechargeable lithium batteries. *Adv. Funct. Mater.* **2005**, *15*, 582–586. [[CrossRef](#)]
130. Lou, X.W.; Wang, Y.; Yuan, C.; Lee, J.Y.; Archer, L.A. Template-free synthesis of SnO<sub>2</sub> hollow nanostructures with high lithium storage capacity. *Adv. Mater.* **2006**, *18*, 2325–2329. [[CrossRef](#)]
131. Yuan, C.; Yang, L.; Hou, L.; Li, J.; Sun, Y.; Zhang, X.; Shen, L.; Lu, X.; Xiong, S.; Lou, X.W. Flexible hybrid paper made of monolayer Co<sub>3</sub>O<sub>4</sub> microsphere arrays on rGO/CNTs and their application in electrochemical capacitors. *Adv. Funct. Mater.* **2012**, *22*, 2560–2566. [[CrossRef](#)]

132. Han, K.; Liu, Z.; Ye, H.; Dai, F. Flexible self-standing graphene–Se@ CNT composite film as a binder-free cathode for rechargeable Li–Se batteries. *J. Power Sources* **2014**, *263*, 85–89. [[CrossRef](#)]
133. Sun, H.; Ahmad, M.; Luo, J.; Shi, Y.; Shen, W.; Zhu, J. SnS<sub>2</sub> nanoflakes decorated multiwalled carbon nanotubes as high performance anode materials for lithium-ion batteries. *Mater. Res. Bull.* **2014**, *49*, 319–324. [[CrossRef](#)]
134. Mia, R.; Sultana, S. Fabrication and properties of silver nanowires (AgNWs) functionalized fabric. *SN Appl. Sci.* **2020**, *2*, 1–15. [[CrossRef](#)]
135. Novák, P.; Müller, K.; Santhanam, K.; Haas, O. Electrochemically active polymers for rechargeable batteries. *Chem. Rev.* **1997**, *97*, 207–282. [[CrossRef](#)] [[PubMed](#)]
136. Wang, C.; Zhang, X.; Qian, Y.; Wu, H.; Kan, E. First-principles study on S and N doping graphene/SnS<sub>2</sub> heterostructure for lithium-ion battery. *Chem. Phys. Lett.* **2021**, *769*, 138391. [[CrossRef](#)]
137. Zhang, M.; Lei, D.; Yu, X.; Chen, L.; Li, Q.; Wang, Y.; Wang, T.; Cao, G. Graphene oxide oxidizes stannous ions to synthesize tin sulfide–graphene nanocomposites with small crystal size for high performance lithium ion batteries. *J. Mater. Chem.* **2012**, *22*, 23091–23097. [[CrossRef](#)]
138. Yin, J.; Cao, H.; Zhou, Z.; Zhang, J.; Qu, M. SnS<sub>2</sub>@reduced graphene oxide nanocomposites as anode materials with high capacity for rechargeable lithium ion batteries. *J. Mater. Chem.* **2012**, *22*, 23963–23970. [[CrossRef](#)]
139. Chang, K.; Wang, Z.; Huang, G.; Li, H.; Chen, W.; Lee, J.Y. Few-layer SnS<sub>2</sub>/graphene hybrid with exceptional electrochemical performance as lithium-ion battery anode. *J. Power Sources* **2012**, *201*, 259–266. [[CrossRef](#)]
140. Wei, W.; Jia, F.-F.; Wang, K.-F.; Qu, P. SnS<sub>2</sub>/graphene nanocomposite: A high rate anode material for lithium ion battery. *Chin. Chem. Lett.* **2017**, *28*, 324–328. [[CrossRef](#)]
141. Wang, H.-E.; Zhao, X.; Li, X.; Wang, Z.; Liu, C.; Lu, Z.; Zhang, W.; Cao, G. rGO/SnS<sub>2</sub>/TiO<sub>2</sub> heterostructured composite with dual-confinement for enhanced lithium-ion storage. *J. Mater. Chem. A* **2017**, *5*, 25056–25063. [[CrossRef](#)]
142. Luo, B.; Fang, Y.; Wang, B.; Zhou, J.; Song, H.; Zhi, L. Two dimensional graphene–SnS<sub>2</sub> hybrids with superior rate capability for lithium ion storage. *Energy Environ. Sci.* **2012**, *5*, 5226–5230. [[CrossRef](#)]
143. Du, N.; Wu, X.; Zhai, C.; Zhang, H.; Yang, D. Large-scale synthesis and application of SnS<sub>2</sub>–graphene nanocomposites as anode materials for lithium-ion batteries with enhanced cyclic performance and reversible capacity. *J. Alloys Compd.* **2013**, *580*, 457–464. [[CrossRef](#)]
144. Ren, Y.; Lv, W.; Wen, F.; Xiang, J.; Liu, Z. Microwave synthesis of SnS<sub>2</sub> nanoflakes anchored graphene foam for flexible lithium-ion battery anodes with long cycling life. *Mater. Lett.* **2016**, *174*, 24–27. [[CrossRef](#)]
145. Zhuo, L.; Wu, Y.; Wang, L.; Yu, Y.; Zhang, X.; Zhao, F. One-step hydrothermal synthesis of SnS<sub>2</sub>/graphene composites as anode material for highly efficient rechargeable lithium ion batteries. *RSC Adv.* **2012**, *2*, 5084–5087. [[CrossRef](#)]
146. Xia, J.; Liu, L.; Xie, J.; Yan, H.; Yuan, Y.; Chen, M.; Huang, C.; Zhang, Y.; Nie, S.; Wang, X. Layer-by-layered SnS<sub>2</sub>/graphene hybrid nanosheets via ball-milling as promising anode materials for lithium ion batteries. *Electrochim. Acta* **2018**, *269*, 452–461. [[CrossRef](#)]
147. Sathish, M.; Mitani, S.; Tomai, T.; Honma, I. Ultrathin SnS<sub>2</sub> nanoparticles on graphene nanosheets: Synthesis, characterization, and Li-ion storage applications. *J. Phys. Chem. C* **2012**, *116*, 12475–12481. [[CrossRef](#)]
148. Tang, H.; Qi, X.; Han, W.; Ren, L.; Liu, Y.; Wang, X.; Zhong, J. SnS<sub>2</sub> nanoplates embedded in 3D interconnected graphene network as anode material with superior lithium storage performance. *Appl. Surf. Sci.* **2015**, *355*, 7–13. [[CrossRef](#)]
149. Jiang, Y.; Song, D.; Wu, J.; Wang, Z.; Huang, S.; Xu, Y.; Chen, Z.; Zhao, B.; Zhang, J. Sandwich-like SnS<sub>2</sub>/graphene/SnS<sub>2</sub> with expanded interlayer distance as high-rate lithium/sodium-ion battery anode materials. *ACS Nano* **2019**, *13*, 9100–9111. [[CrossRef](#)]
150. Jiang, X.; Yang, X.; Zhu, Y.; Shen, J.; Fan, K.; Li, C. In situ assembly of graphene sheets-supported SnS<sub>2</sub> nanoplates into 3D macroporous aerogels for high-performance lithium ion batteries. *J. Power Sources* **2013**, *237*, 178–186. [[CrossRef](#)]
151. Zhang, Q.; Sun, Y.; Zhang, X.; Guo, J. 3D architecture constructed by 2D SnS<sub>2</sub>-graphene hybrids towards large and fast lithium storage. *Mater. Lett.* **2016**, *185*, 311–314. [[CrossRef](#)]
152. Zhang, X.; Xiang, J.; Mu, C.; Wen, F.; Yuan, S.; Zhao, J.; Xu, D.; Su, C.; Liu, Z. SnS<sub>2</sub> nanoflakes anchored graphene obtained by liquid phase exfoliation and MoS<sub>2</sub> nanosheet composites as lithium and sodium battery anodes. *Electrochim. Acta* **2017**, *227*, 203–209. [[CrossRef](#)]
153. Wang, Q.; Nie, Y.-X.; He, B.; Xing, L.-L.; Xue, X.-Y. SnS<sub>2</sub>–graphene nanocomposites as anodes of lithium-ion batteries. *Solid State Sci.* **2014**, *31*, 81–84. [[CrossRef](#)]
154. Jiang, J.; Feng, Y.; Mahmood, N.; Liu, F.; Hou, Y. SnS<sub>2</sub>/graphene composites: Excellent anode materials for lithium ion battery and photolysis catalysts. *Sci. Adv. Mater.* **2013**, *5*, 1667–1675. [[CrossRef](#)]
155. Liu, S.; Lu, X.; Xie, J.; Cao, G.; Zhu, T.; Zhao, X. Preferential c-axis orientation of ultrathin SnS<sub>2</sub> nanoplates on graphene as high-performance anode for Li-ion batteries. *ACS Appl. Mater. Interfaces* **2013**, *5*, 1588–1595. [[CrossRef](#)]
156. Mei, L.; Xu, C.; Yang, T.; Ma, J.; Chen, L.; Li, Q.; Wang, T. Superior electrochemical performance of ultrasmall SnS<sub>2</sub> nanocrystals decorated on flexible RGO in lithium-ion batteries. *J. Mater. Chem. A* **2013**, *1*, 8658–8664. [[CrossRef](#)]
157. Chen, H.; Zhang, B.; Zhang, J.; Yu, W.; Zheng, J.; Ding, Z.; Li, H.; Ming, L.; Bengono, D.; Chen, S. In-situ grown SnS<sub>2</sub> nanosheets on rGO as an advanced anode material for lithium and sodium ion batteries. *Front. Chem.* **2018**, *6*, 629. [[CrossRef](#)] [[PubMed](#)]
158. Kong, D.; He, H.; Song, Q.; Wang, B.; Yang, Q.-H.; Zhi, L. A novel SnS<sub>2</sub>@ graphene nanocable network for high-performance lithium storage. *RSC Adv.* **2014**, *4*, 23372–23376. [[CrossRef](#)]
159. Li, X.; Sun, X.; Gao, Z.; Hu, X.; Ling, R.; Cai, S.; Zheng, C.; Hu, W. A Simple One-Pot Strategy for Synthesizing Ultrafine SnS<sub>2</sub> Nanoparticle/Graphene Composites as Anodes for Lithium/Sodium-Ion Batteries. *ChemSusChem* **2018**, *11*, 1549–1557. [[CrossRef](#)]

160. Yao, J.; Shen, X.; Wang, B.; Liu, H.; Wang, G. In situ chemical synthesis of SnO<sub>2</sub>-graphene nanocomposite as anode materials for lithium-ion batteries. *Electrochem. Commun.* **2009**, *11*, 1849–1852. [[CrossRef](#)]
161. Zhao, B.; Song, D.; Ding, Y.; Li, W.; Wang, Z.; Jiang, Y.; Zhang, J. Size-tunable SnS<sub>2</sub> nanoparticles assembled on graphene as anodes for high performance lithium/sodium-ion batteries. *Electrochim. Acta* **2020**, *354*, 136730. [[CrossRef](#)]
162. Wu, Y.-Q.; Yang, Y.; Pu, H.; Gao, R.-Z.; Meng, W.-J.; Yang, H.-X.; Zhao, D.-L. SnS<sub>2</sub> nanoparticle-integrated graphene nanosheets as high-performance and cycle-stable anodes for lithium and sodium storage. *J. Alloys Compd.* **2020**, *822*, 153686. [[CrossRef](#)]
163. Cheng, M.; Hu, Q.; Du, C.; Li, J.; Liao, W.; Li, J.; Huang, X. An ionic liquid-assisted route towards SnS<sub>2</sub> nanoparticles anchored on reduced graphene oxide for lithium-ion battery anode. *J. Solid State Chem.* **2021**, *296*, 122022. [[CrossRef](#)]
164. Zhong, Y.; Mahmud, S.; He, Z.; Yang, Y.; Zhang, Z.; Guo, F.; Chen, Z.; Xiong, Z.; Zhao, Y. Graphene oxide modified membrane for highly efficient wastewater treatment by dynamic combination of nanofiltration and catalysis. *J. Hazard. Mater.* **2020**, *397*, 122774. [[CrossRef](#)] [[PubMed](#)]
165. Khan, M.T.; Al Mamun, M.A.; Rony, M.; Anchang, X.; Rashid, M.M. Effect of Different Solvent Systems on Fiber Morphology and Property of Electrospun PCL Nano Fibers. *Tekst. Mühendis* **2021**, *28*, 61–76. [[CrossRef](#)]
166. Li, Y.-F.; Wang, S.-G.; Shi, Y.-H.; Fan, C.-Y.; Lin, J.; Wu, X.-L.; Sun, H.-Z.; Zhang, J.-P.; Xie, H.-M. In situ chemically encapsulated and controlled SnS<sub>2</sub> nanocrystal composites for durable lithium/sodium-ion batteries. *Dalton Trans.* **2020**, *49*, 15874–15882. [[CrossRef](#)] [[PubMed](#)]
167. Xu, Y.; Sheng, K.; Li, C.; Shi, G. Self-assembled graphene hydrogel via a one-step hydrothermal process. *ACS Nano* **2010**, *4*, 4324–4330. [[CrossRef](#)] [[PubMed](#)]
168. Zhou, Q.; Li, Y.; Huang, L.; Li, C.; Shi, G. Three-dimensional porous graphene/polyaniline composites for high-rate electrochemical capacitors. *J. Mater. Chem. A* **2014**, *2*, 17489–17494. [[CrossRef](#)]
169. Tang, Z.; Shen, S.; Zhuang, J.; Wang, X. Noble-metal-promoted three-dimensional macroassembly of single-layered graphene oxide. *Angew. Chem.* **2010**, *122*, 4707–4711. [[CrossRef](#)]
170. Zhang, L.; Huang, Y.; Zhang, Y.; Fan, W.; Liu, T. Three-dimensional nanoporous graphene-carbon nanotube hybrid frameworks for confinement of SnS<sub>2</sub> nanosheets: Flexible and binder-free papers with highly reversible lithium storage. *ACS Appl. Mater. Interfaces* **2015**, *7*, 27823–27830. [[CrossRef](#)]